NASA CONTRACTOR REPORT

NASA CR-2236

NASA CR-2236

# RADIATIVE COUPLED VISCOUS FLOW WITH MASSIVE BLOWING

*by Y. S. Chou*

*Prepared by*
LOCKHEED MISSILES & SPACE COMPANY
Sunnyvale, Calif.
*for Ames Research Center*

NATIONAL AERONAUTICS AND SPACE ADMINISTRATION • WASHINGTON, D. C. • MARCH 1973

| 1. Report No. | 2. Government Accession No. | 3. Recipient's Catalog No. |
|---|---|---|
| NASA CR 2236 | | |

| 4. Title and Subtitle | 5. Report Date |
|---|---|
| "Radiative Coupled Viscous Flow with Massive Blowing" | March 1973 |
| | 6. Performing Organization Code |

| 7. Author(s) | 8. Performing Organization Report No. |
|---|---|
| Y.S. Chou | |
| | 10. Work Unit No. |

| 9. Performing Organization Name and Address | 11. Contract or Grant No. |
|---|---|
| Lockheed Missiles & Space Company<br>Sunnyvale, California | NAS 2-6668 |
| | 13. Type of Report and Period Covered |

| 12. Sponsoring Agency Name and Address | 13. Type of Report and Period Covered |
|---|---|
| | Contractor Report |
| National Aeronautics & Space Administration<br>Washington, D.C. | 14. Sponsoring Agency Code |

15. Supplementary Notes

16. Abstract

An analysis of the fully-coupled viscous, radiating flow past an ablating blunt body at hyperbolic entry conditions is presented. A detailed thermodynamics computation, as well as a realistic radiation transport model, is included. A locally nonsimilar approach is employed to solve the conservation equations away from the stagnation point. The validity of the locally nonsimilar approach is demonstrated for some nonablating cases. Sample calculations are made for the typical flight condition of a Jovian entry probe. The effects of the downstream injection of the ablation products of a carbon heat shield on the flux distribution around the body are discussed in detail. It is found that most of the radiative energy is absorbed by the injected carbon gas and dumped into the wake.

| 17. Key Words (Suggested by Author(s)) | 18. Distribution Statement |
|---|---|
| Viscous, Radiation, Heating Ablation, Boundary Layer, Entry, Hypersonic, Planetary | UNCLASSIFIED - UNLIMITED |

| 19. Security Classif. (of this report) | 20. Security Classif. (of this page) | 21. No. of Pages | 22. Price* |
|---|---|---|---|
| UNCLASSIFIED | UNCLASSIFIED | 43 | $3.00 |

* For sale by the National Technical Information Service, Springfield, Virginia 22151

Page Intentionally Left Blank

## ABSTRACT

An analysis of the fully coupled viscous, radiating flow past an ablating blunt body at hyperbolic entry conditions is presented. A detailed thermodynamics computation, as well as a realistic radiation transport model, is included in this analysis. A locally nonsimilar approach is employed to solve the conservation equations away from the stagnation point. The validity of the locally nonsimilar approach is demonstrated for some nonablating cases. Sample calculations are made for the typical flight condition of a Jovian entry probe. The effects of the downstream injection of the ablation products of a carbon heat shield on the flux distribution around the body are discussed in detail. It is found that most of the radiative energy is absorbed by the injected carbon gas and dumped into the wake. **A companion report, (NASA CR-2235) is available of the SL-4 Code and instructions for operation.**

## NOMENCLATURE

| | |
|---|---|
| $B(y,\nu)$ | Planck function |
| $C_v$ | Mass fraction of the ablation gas |
| $C_{v\xi}$ | $\frac{\partial C_v}{\partial \xi}$ |
| $\overline{C}_v$ | $\beta_1 C_{v\xi}$ |
| $D$ | Effective binary diffusion coefficient |
| $D_s(o)$ | Binary diffusion coefficient behind the shock at stagnation point |
| $f$ | $u/u_s$, normalized tangential velocity |
| $f_\xi$ | $\frac{\partial f}{\partial \xi}$ |
| $F$ | $\beta_1 f f_\xi$ |
| $F_r$ | Radiative flux |
| $F_{rw}$ | Radiative flux at wall |
| $F_{rw}(\dot{M}=0)$ | Radiative flux at wall when injection rate is zero |
| $H$ | Total enthalpy, also normalized total enthalpy, normalized by $H_s$ |
| $H_\xi$ | $\frac{\partial H}{\partial \xi}$ |
| $\overline{H}$ | $\beta_1 H_\xi$ |
| $h$ | Static enthalpy, also normalized static enthalpy, normalized by $H_s$ |
| $I(\nu,y,\Omega)$ | Spectral radiation intensity |
| $\tilde{K}$ | $1-k_y$ |
| $k$ | Shock curvature |

| | |
|---|---|
| $\dot{M}$ | Total injected mass flow per unit area as a function of $r_w$ |
| $p$ | Pressure |
| $Pr$ | Prandtl number |
| $Q$ | Radiative flux divergence |
| $r$ | Distance measured from axis of symmetry |
| $R_s$ | Shock radius of curvature at stagnation point |
| $Re$ | Reynolds number $\rho_\infty u_\infty R_s/\mu_s(o)$ |
| $Sc$ | Schmidt number $\mu_s(o)/\rho_\infty D_s(o)$ |
| $T$ | Temperature |
| $T_s(o)$ | Temperature behind the shock at stagnation point |
| $u$ | Tangential velocity, velocity component parallel to the shock |
| $U_\infty$ | Free stream velocity |
| $v$ | Velocity component perpendicular to the shock |
| $x$ | Distance parallel to the shock measured from stagnation line |
| $y$ | Distance normal to the shock |
| $z$ | Distance along the line of symmetry from the shock stagnation point |
| $\mu$ | Viscosity |
| $\mu_s(o)$ | Viscosity behind the shock at stagnation point |
| $\alpha(\nu,y)$ | Absorption coefficient |
| $\alpha_i$ | Elemental gas mass fraction |
| $\beta_1 \cdots \beta_5$ | Parameters defined by Eqs. (11) and (12) |
| $\Delta$ | Shock layer thickness |
| $\xi$ | Transformed variable $\xi = x$ |
| $\eta$ | Normalized stream function defined by Eq. (7) |

| | |
|---|---|
| $\psi$ | Stream function |
| $\epsilon$ | Stagnation point density ratio across the shock |
| $\nu$ | Frequency |
| $\rho$ | Density |
| $\omega$ | Parametric variable defined by Eq. (21) |

Subscripts

| | |
|---|---|
| s | Quantities at shock |
| b | Quantities at body |
| w | Quantities at wall |
| $\infty$ | Freestream conditions |
| $\xi$ | Partial derivative with respect to variable $\xi$ . |

## 1.0 INTRODUCTION

The purpose of the present study is to investigate the effect of surface blowing on the thermal environment of a vehicle entering planetary atmospheres at hyperbolic speed. Most of the earlier studies which included the effect of ablation products are confined to the stagnation region (Refs. 1-5). The only solutions obtained away from the stagnation region appear to be that of Olsted's (Ref. 6). Olsted adapted a two layer inviscid model and treated air to air surface injection only. Since no diffusion mechanism is allowed in the inviscid model, it probably is too crude an approximation for treating the effect of ablation products. In the present report, we study the thin-radiating shock layer about blunt bodies with surface mass injection, and do not restrict the analysis to the stagnation region. Viscous effects, as well as diffusion of the injected materials, will be considered.

In our previous work, reported in Ref. 7, solutions for a thin radiating shock layer about blunt bodies without blowing were obtained by a locally nonsimilar approach. Perfect gas and constant transport properties were assumed and only the continuum radiation was considered. Due to these simplifications, especially the nonblowing restriction, the results were not quantitatively realistic. Validity of the locally nonsimilar approach in solving the thin shock layer problem was sufficiently demonstrated, however. The work reported herein is a continuation of that of Ref. 7. The additional tasks were to incorporate a realistic radiation transport model as well as more detailed thermodynamic properties; to allow the ablation products to diffuse into the shock layer and to rederive the governing equations so that mass injection rates variable with distance around the body could be treated.

The approximate but still complete treatment of the radiative transport in mixtures of hydrogen, helium, carbon, nitrogen and oxygen developed by Wilson (Ref. 5) was adapted to the present work. In this treatment, continuum radiation is approximated by a twenty-six-band model and atomic line radiation is represented by eleven-line groups. The radiation field, i.e., the flux

and its divergence, is determined by the solution to the one-dimensional radiative transfer equation. The validity of using one-dimensional radiative transfer equations for thin shock layer problems has been demonstrated as adequate in Ref. 8.

The shock layer is assumed to be in thermochemical equilibrium. Hence, given pressure, temperature (or enthalpy) and elemental species concentration at any point in the shock layer, other thermodynamic variables can be completely determined by a Free Energy Minimization procedure. This is implemented in the present work by the FEMP Computer Program, described in detail in Ref. 9. Transport properties for a gas mixture, such as viscosity and heat conductivity, are computed by the approximate formulas of Refs. 10 and 11.

The method of solution employed here is an inverse one, that is to say, the shock is completely specified and the body shape is a part of the solution. For a specific body shape, therefore, iterations would have to be performed on the given shock shape. Fortunately, the problems we will be interested in are thin shock layer problems; namely, the shock shape does not deviate much from the body shape. A good first guess on shock shape can be made and iteration largely can be avoided.

Calculations for a body shape and flight condition, which represents a typical entry of a Jupiter probe, were made. The injected gas is assumed to be pure carbon, and the injection rate is a monotonically decreasing function of shock radius. The radiative heating distribution around the body is presented. This distribution is compared with that of no surface mass injection.

## 2.0 MATHEMATICAL DEVELOPMENT

### 2.1 Governing Equations

The conservation equations for an axisymmetric thin shock layer, written in a shock oriented coordinate system (Fig. 1) are:

Continuity
$$\frac{\partial \rho u r}{\partial x} + \frac{\partial \rho v r \tilde{k}}{\partial y} = 0 \tag{1}$$

x-momentum
$$\rho \frac{\partial}{\partial y}\left(\mu \frac{\partial u}{\partial y}\right) - \rho u \frac{\partial u}{\partial x} - \rho v \tilde{k} \frac{\partial u}{\partial y} + \rho k u v - \frac{\partial p}{\partial x} = 0 \tag{2}$$

y-momentum
$$k_s u_s^2 \rho + \frac{\partial p}{\partial y} = 0 \tag{3}$$

energy
$$\frac{\partial}{\partial y}\left[\frac{\mu}{Pr} \frac{\partial H}{\partial y} + \frac{\mu}{2}\left(1-\frac{1}{Pr}\right) \frac{\partial u^2}{\partial y}\right] - \rho u \frac{\partial H}{\partial x} - \tilde{k} \rho v \frac{\partial H}{\partial y} + Q = 0 \tag{4}$$

specie
$$\frac{\partial}{\partial y}\left(\rho D \frac{\partial C_v}{\partial y}\right) - \rho u \frac{\partial C_v}{\partial x} - \tilde{k} \rho v \frac{\partial C_v}{\partial y} = 0 \tag{5}$$

The y-momentum equation, Eq. (3), has been simplified according to Maslen's approximation (Ref. 12). The validity of Maslen's approximation has been examined in Ref. 7. In the energy equation, Eq. (4), the Lewis number is assumed to be unity. The symbol $Q$ represents the radiative flux divergence, the precise form of $Q$ will be discussed in the next section.

In the specie conservation equation, Eq. (5), $C_v$ denotes the mass fraction of the ablation gas. Here we have assumed a binary diffusion process, i.e., the ablation gas diffuses as a whole into the shock heated atmospheric gas. The detailed derivation of Eq. (5) can be found in Ref. 1 or Ref. 4. This binary diffusion model will be valid if the gas mixture can be divided into two groups of species, each with about the same atomic or molecular weight and about the same mutual collision cross section. Otherwise, multicomponent diffusion should be considered. For the sake of simplicity, the binary model was used in this study.

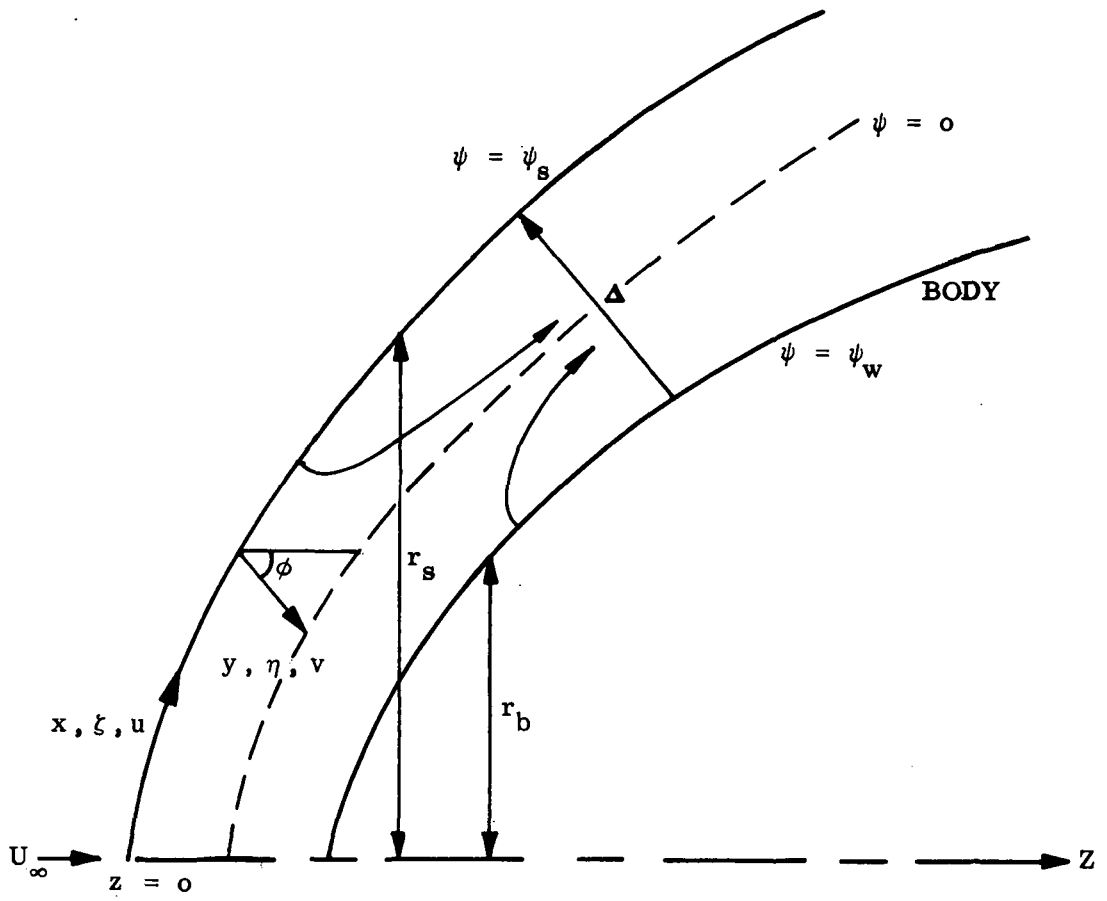


Fig. 1. Sketch of Geometry

Once the mass fraction for ablation gas $C_v$ is known, the mass fraction for elemental gas i is given by

$$\alpha_i = (\alpha_v)_i C_v + (\alpha_a)_i (1-C_v) \tag{6}$$

Where $(\alpha_v)_i$ is the mass fraction of <u>element</u> i in the ablation gas, and $(\alpha_a)_i$ is the mass fraction of element i in the atmospheric gas. Furthermore, given the $\alpha_i$'s, the <u>species</u> mass fraction can be determined by FEMP.

We now proceed to normalize the variables. The distance x,y and the distance from the axis are normalized by the stagnation point shock radius of curvature $R_s$, the velocity u by the freestream velocity $u_\infty$, the density $\rho$ by the freestream density $\rho_\infty$, the pressure p by twice the freestream dynamic pressure $\rho_\infty u_\infty^2$, the shock curvature k by $1/R_s$, the total enthalpy H as well as the static enthalpy h by the total enthalpy immediately behind the shock $H_s$, the stream function $\psi$ by $\rho_\infty u_\infty R_s^2$, the viscosity by its value immediately behind the normal shock $\mu_s(0)$, and finally, the radiative flux Q by

$$\frac{2R_s}{\rho_\infty u_\infty^3}$$

From here on, the equations are all written in nondimensional form.

Let us divide the shock layer into two sublayers, one is the layer dominated by the atmospheric gas where $\psi > 0$. The other is the layer dominated by the ablation gas where $\psi < 0$. We introduce new independent variables $\xi$ and $\eta$, defined as:

$$\xi(x) = x, \qquad \eta(x,y) = \frac{\psi}{\beta_8 r_s^2}, \qquad d\psi = -\rho u r dy + \rho v r \tilde{k} dx \tag{7}$$

where

$$\beta_8 = 1 \quad \text{for} \quad \psi > 0, \qquad \beta_8 = \dot{M} \quad \text{for} \quad \psi < 0$$

$$\dot{M} = -\frac{2\int_0^{r_w} (\rho v)_w r_w dr_w}{r_w^2} \simeq -\frac{2\int_0^{r_s} (\rho v)_w r_s dr_s}{r_s^2} \tag{8}$$

Hence, $\dot{M}$ is the total injected mass flow per unit area as a function of $r_w$. For a thin shock layer we approximate $r_w \simeq r_s$. In Eq. (8), $(\rho v)_w$ is the local injection rate which remains to be specified. (Note that $(\rho v)_w$ will be negative according to the present coordinate system.)

By definition, the stream function at shock is $\psi_s = \frac{1}{2} r_s^2$ and at wall is $\psi_w \simeq \int_0^{r_s} (\rho v)_w r_s dr_s$. Hence the range of our new variable $\eta$ will be from $\frac{1}{2}$ to $-\frac{1}{2}$.

It should be noted that by choosing new variables $\xi$ and $\eta$ the continuity equation, Eq. (1), is satisfied automatically, and the y-momentum equation can be integrated to give the pressure field as

$$p = p_s + (\beta_8 \eta - \tfrac{1}{2}) k_s u_s r_s \tag{9}$$

Let us now define $f \equiv \frac{u}{u_s}$, then, from the x-momentum equation (Eq. (2)), we obtain an equation for $f$ as

$$\frac{f}{2} \frac{\partial}{\partial \eta}\left(\rho\mu \frac{\partial f^2}{\partial \eta}\right) + Re\beta_5^{\pm}\left[\eta \frac{\partial f^2}{\partial \eta} - \beta_1^{\pm} f f_\xi - \beta_2^{\pm}\left(f^2 - \frac{2}{\rho}\right) + \frac{1}{\rho}\left(\beta_4^{\pm} - \eta\beta_3^{\pm}\right)\right] = 0 \tag{10}$$

where $f_\xi \equiv \frac{\partial f}{\partial \xi}$ and the superscript of $(\pm)$ indicates that different $\beta$'s should be used dependent on whether $\eta$ is greater or less than zero. The $\beta$'s are given as the following:

for $\eta \geq 0$

$$\beta_1^+ = r_s \Big/ \frac{dr_s}{d\xi}, \qquad \beta_2^+ = \frac{\beta_1^+}{u_s} \frac{du_s}{d\xi}$$

$$\beta_3^+ = \frac{r_s k_s}{u_s}(\beta_2^+ - 1) + \beta_1^+ \frac{r_s}{u_s} \frac{dk_s}{d\xi}$$

$$\beta_4^+ = \frac{\beta_3^+}{2} + \frac{k_s r_s}{u_s}$$

$$\beta_5^+ = \frac{r_s}{u_s} \frac{dr_s}{d\xi} \tag{11}$$

for $\eta \leq 0$

$$\beta_1^- = \frac{r_s \dot{M}}{\dot{M}\frac{dr_s}{d\xi} + \frac{r_s}{2}\frac{d\dot{M}}{d\xi}} \quad , \qquad \beta_2^- = \frac{\beta_1^-}{u_s}\frac{du_s}{d\xi}$$

$$\beta_3^- = \dot{M}\frac{r_s k_s}{u_s}(\beta_2^- - 1) + \dot{M}\beta_1^- \frac{r_s}{u_s}\frac{dk_s}{d\xi} + \frac{\beta_1^- k_s r_s}{u_s}\frac{d\dot{M}}{d\xi}$$

$$\beta_4^- = \frac{\beta_3^-}{2} + \frac{k_s r_s}{u_s}$$

$$\beta_5^- = \dot{M}^2\beta_5^+ + \frac{\dot{M} r_s^2}{2u_s}\frac{d\dot{M}}{d\xi} \tag{12}$$

Similarly, the energy and specie conservation equations can be written as

$$\frac{\partial}{\partial\eta}\left[\frac{\rho\mu f}{Pr}\frac{\partial H}{\partial\eta}\right] + 2u_s^2\frac{\partial}{\partial\eta}\left[\rho\mu(1-\frac{1}{Pr})f^2\frac{\partial f}{\partial\eta}\right]$$

$$+ Re\beta_5^{\pm}\left[2\eta\frac{\partial H}{\partial\eta} - \beta_1^{\pm}H_\xi - \frac{\beta_1^{\pm}}{\rho f u_s}Q\right] = 0 \tag{13}$$

where Pr is the Prandtl number and Re is the Reynolds number

$$Re = \frac{\rho_\infty u_\infty R_s}{\mu_s(0)} \qquad \text{and} \qquad H_\xi \equiv \frac{\partial H}{\partial\xi}$$

The specie conservation equation becomes

$$\frac{\partial}{\partial\eta}\left[\rho^2 f D\frac{\partial C_v}{\partial\eta}\right] + S_c Re\beta_5^{\pm}\left[2\eta\frac{\partial C_v}{\partial\eta} - \beta_1^{\pm}C_{v\xi}\right] = 0 \tag{14}$$

where $C_{v\xi} \equiv \frac{\partial C_v}{\partial\xi}$ and $D$ is the effective binary diffusion coefficient. An explicit formula for $D$ will be discussed in Section 4. Sc is the Schmit number defined as

$$S_c = \frac{\mu_s(0)}{\rho_\infty D_s(0)}$$

We note that the nonsimilar terms in Eqs. (10), (13) and (14) are $\beta_1^{\pm} f f_\xi$, $\beta_1^{\pm} H_\xi$ and $\beta_1^{\pm} C_{v\xi}$, respectively. Without these terms, Eqs. (10) to (14) become locally similar equations and $\xi$ appears only as a parameter. The concept of the locally nonsimilar approach is to define those nonsimilar terms as new variables and derive equations for them. We thus define

$$F \equiv \beta_1^{\pm} f f_\xi \quad , \quad \bar{H} = \beta_1^{\pm} H_\xi \quad , \quad \bar{C}_v = \beta_1^{\pm} C_{v\xi} \tag{15}$$

Equations for F, $\bar{H}$ and $\bar{C}_v$ are derived in the following manner. For F we first differentiate Eq. (10) with respect to $\xi$, then multiply it by $\beta_1^{\pm}$. An equation for F results. In this equation, however, another nonsimilar term $\beta_1^{\pm} F_\xi$ is introduced. Theoretically one can define this term as another new variable and derive an equation for it. A set of an infinite number of equations will then result. Truncation must therefore be performed in order to obtain a closed set of equations. For the sake of simplicity we will simply neglect the term $\beta_1^{\pm} F_\xi$ in the F equation. We will call this level of approximation the two-equation model. The validity of this two-equation model has been demonstrated partially in Ref. 7. In the present work more comparisons will be made with some available numerical solutions to examine the validity of the two-equation model in treating thin shock layer problems.

Similarly, the equation for $\bar{H}$ is obtained by differentiating Eq. (13) with respect to $\xi$, multiplying it by $\beta_1^{\pm}$ and neglecting the term $\beta_1^{\pm}\bar{H}_\xi$; the equation for $\bar{C}_v$ is obtained by differentiating Eq. (14) with respect to $\xi$, multiplying it by $\beta_1^{\pm}$ and neglecting the term $\beta_1^{\pm}\bar{C}_{v\xi}$. These equations are given as the following

$$f \frac{\partial}{\partial\eta}\left(\rho\mu \frac{\partial F}{\partial\eta}\right) + f\beta_1 \frac{\partial}{\partial\eta}\left[(\rho\mu)_\xi f \frac{\partial f}{\partial\eta}\right] + \left[\frac{F}{f^2} - \frac{\beta_1^{\pm}\beta_{5\xi}^{\pm}}{\beta_5^{\pm}}\right] f \frac{\partial}{\partial\eta}\left(\rho\mu f \frac{\partial f}{\partial\eta}\right)$$

$$+ \mathrm{Re}\,\beta_5^{\pm}\left[2\eta \frac{\partial F}{\partial\eta} - \beta_1^{\pm}\beta_{2\xi}^{\pm}\left(f^2 - \frac{2}{\rho}\right) - 2\beta_2^{\pm}\left(F + \frac{\beta_1^{\pm}\rho_\xi}{\rho^2}\right)\right.$$

$$\left. - \frac{\beta_1^{\pm}\rho_\xi}{\rho^2}\left(\beta_4^{\pm} - \eta\beta_3^{\pm}\right) + \frac{\beta_1^{\pm}}{\rho}\left(\beta_{4\xi}^{\pm} - \eta\beta_{3\xi}^{\pm}\right)\right] = 0 \tag{16}$$

where

$$(\rho\mu)_\xi \equiv \frac{\partial \rho\mu}{\partial \xi} \quad , \qquad \rho_\xi \equiv \frac{\partial \rho}{\partial \xi} \quad , \qquad \beta^{\pm}_{5\xi} = \frac{d\beta^{\pm}_5}{d\xi}$$

$$\beta^{\pm}_{4\xi} = \frac{d\beta^{\pm}_4}{d\xi} \quad , \qquad \beta^{\pm}_{3\xi} = \frac{d\beta^{\pm}_3}{d\xi}$$

$$\frac{\partial}{\partial\eta}\left[\frac{\rho\mu}{Pr}\, f\, \frac{\partial \bar{H}}{\partial\eta}\right] + \frac{\partial}{\partial\eta}\left[\frac{\rho\mu}{Pr}\,\frac{F}{f}\,\frac{\partial H}{\partial\eta}\right] + \beta^{\pm}_1 \frac{\partial}{\partial\eta}\left[\left(\frac{\rho\mu}{Pr}\right)_\xi f\, \frac{\partial H}{\partial\eta}\right]$$

$$+ 4u_s(u_s)_\xi \beta^{\pm}_1 \frac{\partial}{\partial\eta}\left[\rho\mu\left(1-\frac{1}{Pr}\right)f^2\,\frac{\partial f}{\partial\eta}\right] + 2u_s^2\beta^{\pm}_1 \frac{\partial}{\partial\eta}\left[\left(\rho\mu\left(1-\frac{1}{Pr}\right)\right)_\xi f^2\,\frac{\partial f}{\partial\eta}\right]$$

$$+ 2u_s^2 \frac{\partial}{\partial\eta}\left[\rho\mu\left(1-\frac{1}{Pr}\right)F\,\frac{\partial f}{\partial\eta}\right] + 2u_s^2 \frac{\partial}{\partial\eta}\left[\rho\mu\left(1-\frac{1}{Pr}\right)f\,\frac{\partial F}{\partial\eta}\right]$$

$$+ Re\beta^{\pm}_{5\xi}\beta^{\pm}_1\left[2\eta\,\frac{\partial H}{\partial\eta} - \bar{H} - \frac{\beta^{\pm}_1}{\rho f u_s}\,Q\right] + Re\beta^{\pm}_5\left[2\eta\,\frac{\partial \bar{H}}{\partial\eta} - \beta^{\pm}_1\left(\frac{\beta^{\pm}_1}{\rho f u_s}\right)_\xi Q\right] = 0 \qquad (17)$$

$$\frac{\partial}{\partial\eta}\left[\rho^2 Df\,\frac{\partial \bar{C}_v}{\partial\eta}\right] + \frac{\partial}{\partial\eta}\left[\frac{\rho^2 DF}{f}\,\frac{\partial C_v}{\partial\eta}\right] + \beta^{\pm}_1 \frac{\partial}{\partial\eta}\left[(\rho^2 D)_\xi f\,\frac{\partial C_v}{\partial\eta}\right]$$

$$+2ScRe\,\beta^{\pm}_5\eta\,\frac{\partial \bar{C}_v}{\partial\eta} + ScRe\,\beta^{\pm}_1\beta^{\pm}_{5\xi}\left[2\eta\,\frac{\partial C_v}{\partial\eta} - \bar{C}_v\right] = 0 \qquad (18)$$

In Eq. (17) the further approximation of neglecting $\frac{\partial Q}{\partial \xi}$ has been made. The explicit formula for the radiative flux divergence will be given in Section 3. Needless to say, it will be a strong function of the absorption coefficients. To evaluate $\frac{\partial Q}{\partial \xi}$ requires the $\xi$-derivative of the absorption coefficients. Since a multiband model of the continuum and atomic line radiation are being treated, it would have been extremely complicated to obtain the $\xi$-derivative of the absorption coefficients. By neglecting $\frac{\partial Q}{\partial \xi}$, we greatly simplify

the analysis. An examination of this simplification in terms of the effect of $\frac{\partial Q}{\partial \xi}$ on the radiative wall flux is considered in Section 5.

Equations (10), (13), (14), (16), (17) and (18) provide six equations for f, H, $C_v$ F, $\bar{H}$, $\bar{C}_v$ , six unknowns. These equations can be considered as ordinary differential equations with $\xi$ as a parameter and their solutions can be sought locally. They are fully coupled with the radiation field, the mixture thermodynamics and the mixture transport properties. Methods of computing the radiation field and the thermodynamics will be described in the next two sections.

## 2.2 Boundary Conditions

The boundary conditions for f, H, $C_v$, F, $\bar{H}$ and $\bar{C}_v$ should be given both at wall and at shock. By the definition of f and F , it is clear that at shock f = 1 and F = 0. At the wall, a no slip condition holds for the high Reynolds number cases of interest. Hence, we find that f = 0 and F = 0. We will assume that the shock itself is not radiating and the precursor radiation is negligible, then at shock H = 1 and $\bar{H}$ = 0. At the wall the enthalpy is assumed to be given. Thus $H = H_w$ and $\bar{H} = \bar{H}_w$. Again, due to the high Reynolds numbers of interest, the diffusion layer will be much thinner than the shock layer. Unless the injection rate is extremely high such that the viscous layer is pushed outward near the shock, one would expect that no ablation gas will reach the shock. Assuming the injection rate $(\rho v)_w$ is order of $\rho_\infty u_\infty$ , then at shock $C_v$= 0 and $\bar{C}_v$ = 0.

At the wall, the diffusion current for the mass fraction of the atmospheric gas must exactly equal the convection current of the mass fraction of the atmospheric gas created by the surface mass injection. Hence, at wall we have the relation (in dimensionless form) $\rho D \frac{\partial C_a}{\partial y} = (\rho v)_w C_a ReSc$ where $C_a$ is the mass fraction of atmospheric gas. Note that $C_a = 1-C_v$. We have, in the $\eta$ coordinate, the boundary condition at wall for $C_v$ as

$$f\rho^2 D \frac{\partial C_v}{\partial \eta} = \frac{\dot{M} r_s ReSc}{u_s} (\rho v)_w (1-C_v) \qquad (19)$$

The condition at wall for $\bar{C}_v$ is found by simply differentiating (19) by $\xi$ then multiplying by $\beta_1^-$. We obtain

$$f\rho^2 D \frac{\partial \bar{C}_v}{\partial \eta} = - \frac{ReSc\dot{M}(\rho v)_w r_s}{u_s} + \beta_1^- ReSc\left(\frac{\dot{M}(\rho v)_w r_s}{u_s}\right)_\xi (1-C_v)$$

$$-\left[\frac{F}{f}\rho^2 D + f\beta_1^-(\rho^2 D)_\xi\right]\frac{\partial C_v}{\partial \eta} \qquad (20)$$

## 2.3 Method of Solution

In attempting to solve Eqs. (10)-(18), it was found convenient to transform the independent variable from $\eta$ to a new coordinate

$$\frac{d\eta}{\partial \omega} = \omega_s f\rho\mu \qquad (21)$$

where $\omega$ is assigned the value zero at the wall and unity at the shock.

From Eq. (21) we obtain

$$\eta = \omega \int_0 f\rho\mu d\omega - \tfrac{1}{2} \qquad (22)$$

therefore

$$\omega_s = \frac{1}{\int_0^1 f\rho\mu d\omega} \qquad (23)$$

We define the point $\omega = \omega_o$ as the value of $\omega$ at $\eta = 0$. Then the atmospheric gas layer as defined before extends from $\omega = \omega_o$ to $\omega = 1$. The injected gas layer extends from $\omega = \omega_o$ to $\omega = 0$. The integration of Eqs. (10)-(18) was performed in two different directions from $\omega_o$ toward 1 ($\beta^+$'s are to be used) and from $\omega$ to 0 ($\beta^-$'s are to be used). The conditions at the junction $\omega = \omega_o$ were determined by requiring that the values of f, F, H, $\bar{H}$, $C_v$, $\bar{C}_v$ and their slope in the physical plane be continuous. Hence we require $\frac{\partial f}{\partial y}$, $\frac{\partial F}{\partial y}$, $\frac{\partial H}{\partial y}$, $\frac{\partial C_v}{\partial y}$, $\frac{\partial \bar{H}}{\partial y}$ and $\frac{\partial \bar{C}_v}{\partial y}$ be continuous at $\omega = \omega_o$.

After Eqs. (10) to (18) were transformed with $\omega$ as the independent variable and the junction conditions applied, the following formal solutions were obtained.

For velocity:

$$f^{\pm} = G_1^{\pm}(\omega) + C_f^{\pm} G_2^{\pm}(\omega) + f(\omega_o) \tag{24}$$

$$f = f^{+} \text{ when } \omega_o < \omega < 1 , \quad f = f^{-} \text{ when } 0 \le \omega \le \omega_o$$

with

$$G_1^{\pm}(\omega) = \mathrm{Re}\beta_5^{\pm}\omega_s^2 \int_{\omega_o} d\omega \int_{\omega_o}^{\omega'} e^{-2\mathrm{Re}\beta_5^{\pm}\omega_s \int_{\omega'}^{\omega} \eta d\omega''} \rho\mu \left[ F + \beta_2^{\pm}\left(f^2 - \frac{2}{\rho}\right) - \frac{\beta_4^{\pm} - \eta\beta_3^{\pm}}{\rho} \right] d\omega$$

$$G_2^{\pm}(\omega) = \int_{\omega_o} e^{-2\mathrm{Re}\beta_5^{\pm}\omega_s \int_{\omega_o} \eta d\omega'} d\omega$$

$$f(\omega_o) = \frac{[1 - G^{+}(1)]G_2^{-}(0)\dot{M} + G_2^{+}(1)G_1^{-}(0)}{\dot{M}G_2^{-}(0) - G_2^{+}(1)}$$

$$C_f^{+} = \frac{1 - f(\omega_o) - G_1^{+}(1)}{G_2^{+}(1)} , \qquad C_f^{-} = \dot{M}C_f^{+}$$

For enthalpy profile:

$$H^{\pm} = G_3^{\pm}(\omega) - G_4^{\pm}(\omega) + C_H^{\pm} G_5^{\pm}(\omega) + H(\omega_o) \tag{25}$$

$$H = H^{+} \text{ when } \omega_o \le \omega \le 1 , \qquad H = H^{-} \text{ when } 0 \le \omega \le \omega_o$$

with

$$G_3^{\pm}(\omega) = \int_{\omega_o} \mathrm{Pr} d\omega \int_{\omega_o}^{\omega'} e^{-2\mathrm{Re}\beta_5^{\pm}\omega_s \int_{\omega'}^{\omega} \mathrm{Pr}\eta d\omega''} \left\{ \mathrm{Re}\beta_5^{\pm}\omega_s \left( \omega_s \rho\mu f\bar{H} + \frac{\omega_s \mu \beta_1^{\pm} Q}{u_s} + 4u_s^2 \eta(\mathrm{Pr}-1) f \frac{\partial f}{\partial \omega'} \right) \right\} d\omega'$$

$$G_4^{\pm}(\omega) = 2u_s^2 \int_{\omega_o} (\mathrm{Pr}-1) f \frac{\partial f}{\partial \omega} d\omega$$

$$G_5^{\pm}(\omega) = \int_{\omega_o} \Pr\, e^{-2Re\beta_5^{\pm}\omega_s \int_{\omega_o}^{} \Pr\eta d\omega}\, d\omega$$

$$H(\omega_o) = \frac{G_5^+(1)[H_w - G_3^-(0) + G_4^-(0)] - G_5^-(0)[1-G_3^+(1) + G_4^+(1)]\dot{M}}{G_5^+(1) - G_5^-(0)\dot{M}}$$

$$C_H^+ = \frac{1-G_3^+(1) + G_4^+(1) - H(\omega_o)}{G_5^+(1)} \qquad C_H^- = \dot{M}C_H^+$$

For specie profiles

$$C_v^{\pm} = G_6^{\pm}(\omega) + C_c^{\pm}G_7^{\pm}(\omega) + C_v(\omega_o) \tag{26}$$

$$C_v = C_v^+ \text{ when } \omega_o \le \omega \le 1 \quad , \qquad C_v = C_v^- \text{ when } 0 \le \omega \le \omega_o$$

with

$$G_6^{\pm} = \omega_s^2 ScRe\beta_5^{\pm} \int_{\omega_o} \frac{\mu}{\rho D} d\omega \int_{\omega_o} e^{-2ScRe\beta_5^{\pm}\omega_s \int_{\omega'}^{\omega} \frac{\mu}{\rho D}\eta d\omega''} f\rho\mu\bar{C}_v d\omega'$$

$$G_7^{\pm}(\omega) = \int_{\omega_o} \frac{\mu}{\rho D}\, e^{-2ScRe\beta_5^{\pm} \int_{\omega_o}^{} \frac{\mu}{\rho D}\eta d\omega'}\, d\omega$$

$$C_v(\omega_o) = \frac{G_7^+ \left.\frac{\partial G_6^-}{\partial \omega}\right)_o - \dot{M}G_6^+ \left.\frac{\partial G_7^-}{\partial \omega}\right)_o - \frac{\omega_s\mu}{\rho D}\frac{\dot{M}ReScr_s}{u_s}(\rho v)_w\left[G_7^+(1) - G_7^+(1)G_6^-(0) + \dot{M}G_6^+(1)G_7^-(0)\right]}{\dot{M}\left.\frac{\partial G_7^-}{\partial \omega}\right)_o + \frac{\omega_s\mu}{\rho D}\frac{\dot{M}ReScr_s}{u_s}(\rho v)_w\left[G_7^-(0)\dot{M} - G_7^+(1)\right]}$$

and

$$C_c^+ = -\frac{G_6^+(1) + C_v(\omega_o)}{G_7^+(1)} \quad , \qquad C_c^- = \dot{M}C_c^+$$

Similar expressions can be obtained for $\bar{H}$, F and $\bar{C}_v$ as follows

$$F^{\pm} = G_8^{\pm}(\omega) + G_9^{\pm}(\omega) + C_F^{\pm} G_{10}^{\pm}(\omega) + F(\omega_o) \tag{27}$$

$$F = F^{+} \text{ when } \omega_o \le \omega \le 1 \quad , \qquad F = F^{-} \text{ when } 0 \le \omega \le \omega_o$$

$$G_8^{\pm}(\omega) = - \beta_1^{\pm} \int_{\omega_o}^{\omega} f \frac{(\rho\mu)_\xi}{\rho\mu} \frac{\partial f}{\partial \omega} \, d\omega$$

$$G_9^{\pm}(\omega) = \int_{\omega_o}^{\omega} f d\omega \int_{\omega_o}^{\omega} e^{-2\omega_s Re \beta_5^{\pm} \int_{\omega'}^{\omega} \eta d\omega} \left\{ 2\omega_s Re \beta_5^{\pm} \beta_1^{\pm} \eta \frac{(\rho\mu)_\xi}{\rho\mu} \frac{\partial f}{\partial \omega} \right.$$

$$+ \left[ \frac{\beta_1^{\pm} \beta_{5\xi}^{\pm}}{\beta_5^{\pm}} - \frac{F}{f^2} \right] \frac{\partial^2 f}{\partial \omega^2} + \omega_s^2 \rho\mu Re \beta_5^{\pm} \left[ \beta_1^{\pm} \beta_{2\xi}^{\pm} \left( f^2 - \frac{2}{\rho} \right) + 2\beta_2^{\pm} \left( F + \frac{\beta_1^{\pm} \rho_\xi}{\rho^2} \right) \right.$$

$$\left. \left. + \frac{\beta_1^{\pm} \rho_\xi}{\rho^2} \left( \beta_4^{\pm} - \eta \beta_3^{\pm} \right) - \frac{\beta_1^2}{\rho} \left( \beta_{4\xi}^{\pm} - \eta \beta_{3\xi}^{\pm} \right) \right] \right\} d\omega'$$

$$G_{10}^{\pm} = \int_{\omega_o}^{\omega} f \, e^{-2\omega_s Re \beta_5^{\pm} \int_{\omega_o}^{\omega} \eta d\omega} \, d\omega$$

$$F(\omega_o) = \frac{G_{10}^{-}(0)\dot{M}[G_8^{+}(1) + G_9^{+}(1)] - G_{10}^{+}(1)[G_8^{-}(0) + G_9^{-}(0)]}{G_{10}^{+}(1) - G_{10}^{-}(0)\dot{M}}$$

$$C_F^{+} = - \frac{G_8^{+}(1) + G_9^{+}(1) + F(\omega_o)}{G_{10}^{+}(1)} \quad , \qquad C_F^{-} = \dot{M} C_F^{+}$$

$$\bar{H}^{\pm} = G_{10}^{\pm}(\omega) + G_{12}^{\pm}(\omega) + C_{\bar{H}}^{\pm} G_{13}^{\pm}(\omega) + \bar{H}(\omega_o) \tag{28}$$

$$\bar{H} = \bar{H}^{+} \text{ when } \omega_o \le \omega \le 1 \quad , \qquad \bar{H} = \bar{H}^{-} \text{ when } 0 \le \omega \le \omega_o$$

with

$$G_{11}^{\pm} = -\int I_1(\omega)d\omega$$

$$I_1(\omega) = \frac{F}{f^2}\frac{\partial H}{\partial \omega} + 2u_s^2(Pr-1)\left(\frac{F}{f}\frac{\partial f}{\partial \omega} + \frac{\partial F}{\partial \omega}\right) + \beta_1\left[\left(\frac{\rho\mu}{Pr}\right)_\xi \frac{Pr}{\rho\mu}\frac{\partial H}{\partial \omega}\right.$$

$$\left. + 4u_s u_{s\xi} f(Pr-1)\frac{\partial f}{\partial \omega} + 2u_s^2 f \frac{Pr}{\rho\mu}\left(\rho\mu\left(1-\frac{1}{Pr}\right)\right)_\xi \frac{\partial f}{\partial \omega}\right]$$

$$G_{12}^{\pm}(\omega) = \int_{\omega_o} Prd\omega \int_{\omega_o} e^{-2Re\beta_5^{\pm}\omega_s\int_{\omega'}^{\omega} Pr\eta d\omega''} I_2(\omega')d\omega'$$

$$I_2(\omega') = 2Re\beta_5^{\pm}\omega_s\eta I_1(\omega') - 2Re\beta_{3\xi}^{\pm}\beta_1^{\pm}\omega_s\eta\frac{\partial H}{\partial \omega} + Re\beta_1^{\pm}\omega_s f\rho\mu\left[\beta_{5\xi}^{\pm}\bar{H} + \left(\frac{\beta_1^{\pm}\beta_{5\xi}^{\pm}}{\rho f u_s}\right)_\xi Q\right]$$

$$G_{13}^{\pm} = \int_{\omega_o} Pr\, e^{-2Re\beta_5^{\pm}\omega_s\int_{\omega_o}\eta Prd\omega} d\omega$$

$$\bar{H}(\omega_o) = \frac{G_{13}^{+}(1)[\bar{H}_w - G_{11}^{-}(0) - G_{12}^{-}(0)] + G_{10}^{-}(0)[G_{11}^{+}(1)+G_{12}^{+}(1)]\dot{M}}{G_{13}^{+}(1) - G_{13}^{-}(0)\dot{M}}$$

$$C_{\bar{H}}^{-} = C_{\bar{H}}^{+}\dot{M} \quad , \qquad C_{\bar{H}}^{+} = -\frac{G_{11}^{+}(1) + G_{12}^{+}(1) + \bar{H}(\omega_o)}{G_{13}^{+}(1)}$$

Finally

$$\bar{C}_v^{\pm} = G_{14}^{\pm}(\omega) + G_{15}^{\pm}(\omega) + C_c^{\pm}\, G_{16}^{\pm}(\omega) + \bar{C}_v(\omega_o) \qquad (29)$$

$$\bar{C}_v = \bar{C}_v^{+} \text{ when } \omega_o \le \omega \le 1 \quad , \qquad \bar{C}_v = \bar{C}_v^{-} \text{ when } 0 \le \omega \le \omega_o$$

with

$$G_{14}^{\pm} = -\int_{\omega_o} \left[ \frac{F}{f^2} + \beta_1^{\pm} \frac{(\rho^2 D)_\xi}{\rho^2 D} \right] \frac{\partial C_v}{\partial \omega} \, d\omega$$

$$G_{15}^{\pm} = \int_{\omega_o} \frac{\mu}{\rho D} \, d\omega \int_{\omega_o} e^{-2ReSc\beta_5^{\pm}\omega_s \int_{\omega'}^{\omega'} \frac{\mu}{\rho D} \eta d\omega''} ReSc\omega_s \left[ 2\beta_5^{\pm}\eta \left( \frac{F}{f^2} + \beta_1^{\pm} \frac{(\rho^2 D)_\xi}{\rho^2 D} \right) \frac{\partial C_v}{\partial \omega} \right.$$

$$\left. - \beta_1^{\pm}\beta_{5\xi}^{\pm} \left( 2\eta \frac{\partial C_v}{\partial \omega} - \omega_s f \rho \mu \bar{C}_v \right) \right] d\omega'$$

$$G_{16}^{\pm} = \int_{\omega_o} \frac{\mu}{\rho D} \, e^{-2ReSc\beta_5^{\pm}\omega_s \int_{\omega_o} \frac{\mu}{\rho D} \eta d\omega} \, d\omega$$

$$\bar{C}_v(\omega_o) = \left\{ G_{16}^{\pm}(1) \left[ \frac{ReSc\dot{M}(\rho v)_w r_s \omega_s}{u_s} \left( G_{14}^{-}(0) + G_{15}^{-}(0) \right) + \frac{\rho D}{\mu} \frac{\partial G_{15}^{-}}{\partial \omega} \right)_o - \beta_1^{-} ReSc\omega_s \left( \frac{\dot{M}(\rho v)_w r_s}{u_s} \right)_\xi \left( 1 - C_v(0) \right) \right]$$

$$- \dot{M} \left( G_{14}^{+}(1) + G_{15}^{+}(1) \right) \left[ \frac{\rho D}{\mu} \frac{\partial G_{16}^{-}}{\partial \omega} \right)_o + \frac{ReSc\dot{M}(\rho v)_w r_s \omega_s}{u_s} G_{16}^{-}(0) \left] \right\} \Bigg/ \left\{ \dot{M} \frac{\rho D}{\mu} \frac{\partial G_{16}^{-}}{\partial \omega} \right)_o$$

$$+ \frac{ReSc\dot{M}(\rho v)_w r_s \omega_s}{u_s} \left( \dot{M} G_{16}^{-}(0) - G_{16}^{+}(1) \right) \Bigg\}$$

The formal solutions given by Eqs. (24)-(29) are in fact integral equations. All the G's are integrals and their integrands are functions of the unknowns f, H, $C_v$, F, $\bar{H}$, $\bar{C}_v$; the thermodynamics and the radiative flux divergence $\bar{Q}$. The advantages of writing the governing equations into the form of Eqs. (24)-(29) are the following: First, the boundary conditions are satisfied exactly by Eqs. (24)-(29). Second, Eqs, (24) to (29) can be solved by iteration. The iteration scheme is more stable than the integration of a second order differential equation with two point boundary conditions.

To solve Eqs. (24)-(29) we first guess profiles for f, H, $C_v$, F, $\bar{H}$ and $\bar{C}_v$. Then, from the thermodynamics subroutine, we obtain the thermodynamic properties as well as the transport properties: density, temperature, species concentration, viscosity, Prandtl number, and diffusion coefficient. With this complete thermodynamic information, the radiative transport subroutine will provide the radiative flux divergence Q. Also, once f, $\rho$, $\mu$ are known, $\omega_s$, $\omega_o$, as well as $\eta$ can be determined. Consequently, all the G functions can be evaluated and a new (i.e., calculated) value for f, H, $C_v$, F, $\bar{H}$, $\bar{C}_v$ obtained. These calculated profiles will then be compared with the guessed ones. If the profiles do not agree within a specified convergence criterion, new profiles will be chosen and the iteration continued until the profiles hopefully converge to a solution.

## 3.0 RADIATION TRANSPORT

The radiation transport model employed in this study is that of Wilson (Refs. 4 and 5). In those references, both the continuum and atomic line transport are considered for a system consisting of H, He C, N, O atoms and significant molecular species. Since helium has high energy level, few helium atoms will be excited in the present shock layer problem; their contribution to the total radiative flux will be small. The presence of helium, however, will affect the composition of gas mixture. Hence, the radiation field will be affected by the presence of helium only through the thermodynamics.

The detailed analysis of Wilson's radiation transport model can be found in Ref. 4. We will not reproduce it here, but will only briefly outline the model below.

It is the radiative flux and the flux divergence that are of interest to us. By definition, they are given as:

$$F_r = \int_0^\infty \int_{\Omega=4\pi} I(y,\nu,\Omega)\cos\theta \, d\Omega d\nu \tag{30}$$

$$Q \equiv \nabla \cdot F_r = \int_0^\infty \int_{\Omega=4\pi} \mu(y,\nu)[I(y,\nu,\Omega) - B(y,\nu)]d\Omega d\nu \tag{31}$$

Where $I(y,\nu,\Omega)$ is the monochromatic intensity at frequency $\nu$ and in the direction $\Omega$, $B(y,\nu)$ is the Planck function. For the present thin shock layer problem, the radiation field is assumed to be one-dimensional. The intensity $I(y,\nu,\Omega)$ can therefore be determined from the one-dimensional radiative transfer equations. They are given as: (with the help of the exponential approximation

$$I^+(\nu,y) = \int_0^y \mu(\nu,y)B(\nu,y')e^{-\ell \int_{y'}^{y} \mu(\nu,y'')dy''} dy'$$

$$I^{-}(\nu,y) = \int_{y}^{\Delta} \mu(\nu,y')B(\nu,y')e^{-\ell\int_{y'}^{y}\mu(\nu,y'')dy''} dy'$$

Where $I^{+}$ is the intensity in the positive $y$ direction and $I^{-}$ in the negative $y$ direction. $\Delta$ is the dimensional shock layer thickness, $\ell$ is the reciprocal direction cosine, and $\mu(\nu,y)$ the absorption coefficient. With a given thermodynamic field and $\mu(\nu,y)$, the intensity field can be determined.

The absorption coefficient is separated into continuum and line contributions.

$$\mu(\nu,y) = \mu^{c}(\nu,y) + \mu^{L}(\nu,y)$$

The flux may then be expressed as the sum of a contribution due to continuum only process $F_r^c$ and a contribution due to lines but corrected by continuum attenuation.

$$F_r = F_r^c + F_r^L \tag{32}$$

with

$$F_r^c = \pi\int_0^{\infty}\left\{\int_0^{E(0,y)} B(\nu,y')dE_{\nu}(y,y') - \int_0^{E(y,\Delta)} B(\nu,y')dE(y,y')\right\} d\nu \tag{33}$$

where the emissive function $E_{\nu}(y,y')$ is defined as

$$E_{\nu}(y,y') = 1 - \exp[\ell\int_{y'}^{y}\mu^{c}(\nu,y'')dy'']$$

and

$$F_r^L = \pi \sum_{\substack{\text{all lines}\\ i}} \left\{\int_0^{W_i(0,y)} B_i(y')dW_i(y'y) - \int^{W_i(y,\Delta)} B_i(y')dW(yy')\right\} \tag{34}$$

where the equivalent width $W_i(y\,y')$ is defined as

$$W_i(yy') = e^{-\ell\int_{y'}^{y}\mu_i^{c}(y'')dy''} \int_{\Delta\nu} [1-\exp(\ell\int_{y'}^{y}\mu_i^{L}(\nu y'')dy'')]\, d\nu$$

Similarly, we can write the flux divergence $Q$ into two parts

$$Q \equiv \nabla \cdot F_r = Q^C + Q^L \tag{35}$$

where

$Q^C$ is the energy emitted and absorbed by the continuum

$$Q^C = 2\pi \int_0^\infty \mu^c(y) \left\{ \int_0^{E_\nu(0,y)} B(\nu,y')dE_\nu(yy') + \int^{E(y,\Delta)} B(\nu,y')dE_\nu(yy') - 2B(\nu,y) \right\} d\nu \tag{36}$$

and

$Q^L$ is the energy emitted and absorbed by the lines. $Q^L$ is computed by numerical differentiation of the line flux $F_r^L$.

The remaining task is to determine the continuum absorption coefficient $\mu^c(\nu,y)$ and the line absorption coefficient $\mu^L(\nu,y)$ for a particular gas mixture. In Ref. 5, twenty-six-band-grey absorption coefficient is modeled for the continuum, and eleven "effective lines" are treated for each atom. The detailed frequency range and their expressions for the continuum absorption and the definition of "effective line" as well as their frequency ranges will not be given here. They are listed in Refs. 4 and 5.

## 4.0 THERMODYNAMIC AND TRANSPORT PROPERTIES

### 4.1 Thermodynamic Properties

Thermodynamic variables such as density, temperature and species concentrations are needed at each point of the shock layer to solve the conservation equations and to calculate the radiative flux. Hence, a relation between these variables and the pressure, enthalpy and elemental mass fraction is required. For a reacting gas mixture, simple state equations are not available. A complete thermochemical equilibrium calculation is necessary to provide the needed thermodynamic properties. A free energy equilibrium program (FEMP) is therefore incorporated in our computer code as a subroutine to provide thermodynamic information. The analysis underlying this program is described in Ref. 9. The original version of FEMP as described in Ref. 9 does not give thermodynamic derivatives. In the present study, certain thermodynamic derivatives are required to provide the $\xi$-derivatives of the thermodynamic variables involved in the governing equations. For example, $\rho_\xi$ appeared in Eq. (16). Applying the chain rule, we can write this derivative as

$$\rho_\xi = \frac{\partial \rho}{\partial \xi} = \frac{\partial \rho}{\partial p}\frac{\partial p}{\partial \xi} + \frac{\partial \rho}{\partial h}\frac{\partial h}{\partial \xi} + \sum_i \frac{\partial \rho}{\partial \alpha_i}\frac{\partial \alpha_i}{\partial \xi} \tag{37}$$

where $\alpha_c$ is the mass fraction of elemental gas $i$.

Equation (37) indicates that we need $\left.\frac{\partial \rho}{\partial p}\right)_{h,\alpha_i}$, $\left.\frac{\partial \rho}{\partial h}\right)_{p,\alpha_i}$ and $\left.\frac{\partial \rho}{\partial \alpha_i}\right)_{p,h}$ We have extended the original FEMP code so that, upon input of p,h and elemental gas mass fraction $\alpha_i$, we obtain not only the thermodynamic variables but also the thermodynamic derivatives.

### 4.2 Transport Properties

Similar to Ref. 4, simplified transport equations of Ref. 10 and 11 have also been used in this study. The approximate viscosity of a gas mixture is given by

$$\mu = \sum_i \frac{\chi_i \mu_i}{\sum_j \chi_j \varphi_{ij}} \tag{38}$$

where $\chi_i$ is the mole fraction and $\mu_i$ is the viscosity of the species $i$.

and

$$\varphi_{ij} = \frac{1}{2\sqrt{2}}\left(1 + \frac{M_i}{M_j}\right)^{-\frac{1}{2}}\left[1 + \left(\frac{\mu_i}{\mu_j}\right)^{\frac{1}{2}}\left(\frac{M_j}{M_i}\right)^{\frac{1}{4}}\right]^2$$

The total thermal conductivity can be written as

$$k_T = \sum_i \frac{\chi_i k_i}{\sum_j \chi_j \varphi_{ij}} + \sum_i Dh_i \frac{\partial C_i}{\partial T} \tag{39}$$

where $D$ is the effective binary diffusion coefficient and $h_i$ is the enthalpy of the species $i$.

The specific heat at constant pressure of the mixture is

$$C_p = \sum_i \left(\overline{C}_{pi} + h_i \frac{\partial C_i}{\partial T}\right) \tag{40}$$

where $\overline{C}_{pi}$ is the frozen specific heat of each species. For air, Blake (Ref. 13) has shown that those approximate equations are valid up to temperatures of 10,000°K.

The temperature dependent diffusion coefficient $D$ used for the C, H, N, O system was that selected by Hoshizaki and Lasher (Ref. 1). This curve-fitted diffusion coefficient may not be adequate when helium is included in the system. The effect of this uncertainty on the radiative wall flux has not been evaluated.

## 5.0 RESULTS

### 5.1 Comparisons with Other Solutions

In order to examine the validity of present locally nonsimilar solutions for thin snock layers, we will make comparisons with other available solutions. Unfortunately there is no solution with massive blowing available for comparison. The important question of the validity of the locally nonsimilar solution for shock layer with mass injection is therefore yet to be answered.

The following comparisons are made:

(a) Adiabatic inviscid flow behind a 45° blunted conic shock is compared with Olstad's solution (Ref. 6).

(b) Adiabatic inviscid flow behind a parabolic shock at high Mach number is compared with a solution by Schneider (Ref. 14), and

(c) Viscous, nonradiating flow over a paraboloid at high Mach and high Reynolds number is compared with the boundary layer solution by Davis and Flugge-Lutz (Ref. 15). All these comparisons are based on perfect gas. The results of the comparisons are present in Fig. 2-5. In Fig. 2, the tangential velocity profiles across the shock layer behind the 45° conic shock are shown at various locations downstream. In Fig. 3, the body shapes behind the parabolic shock are shown. In Fig. 4, the tangential velocity, pressure, as well as the density profiles at z = 10, are shown. Figure 5 shows the convective heat flux and the skin friction distribution around the paraboloid. From these comparisons it seems that the validity of the present locally nonsimilar solution for nonradiating nonblowing thin shock layers has been sufficiently demonstrated.

### 5.2 Viscous Shock Layer with Blowing--but without Radiation

We present here a typical solution for viscous nonradiating flow behind a blunted 45° conic shock with variable surface mass injection. The purpose of presenting this solution is to examine the change of velocity and enthalpy

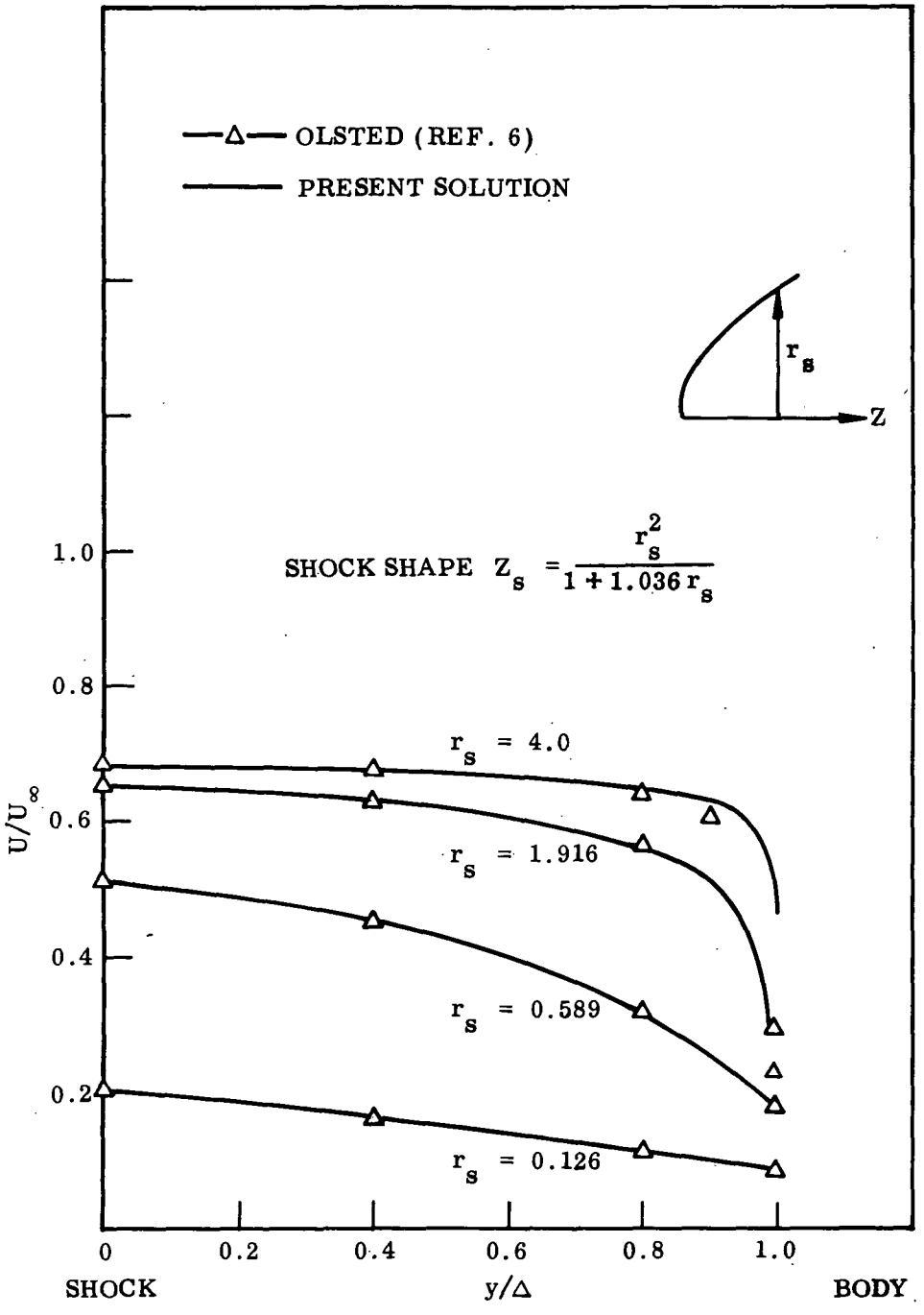


Fig. 2. Inviscid Adiabatic Velocity Profiles for Shock Layer Behind a 45° Conical Shock

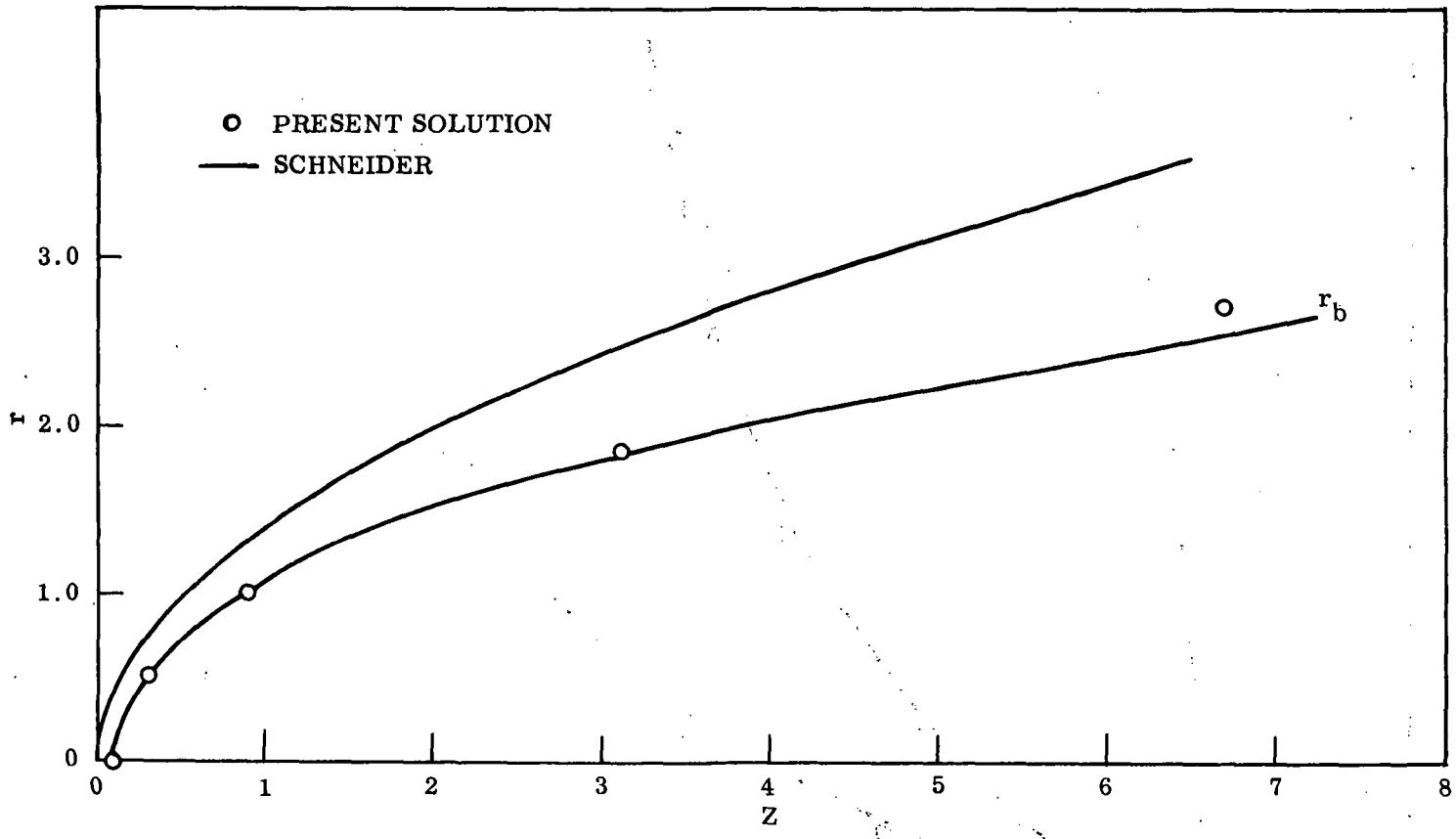


Fig. 3. Inviscid Adiabatic Body Shape Behind a Parabolic Shock at Mach ∞

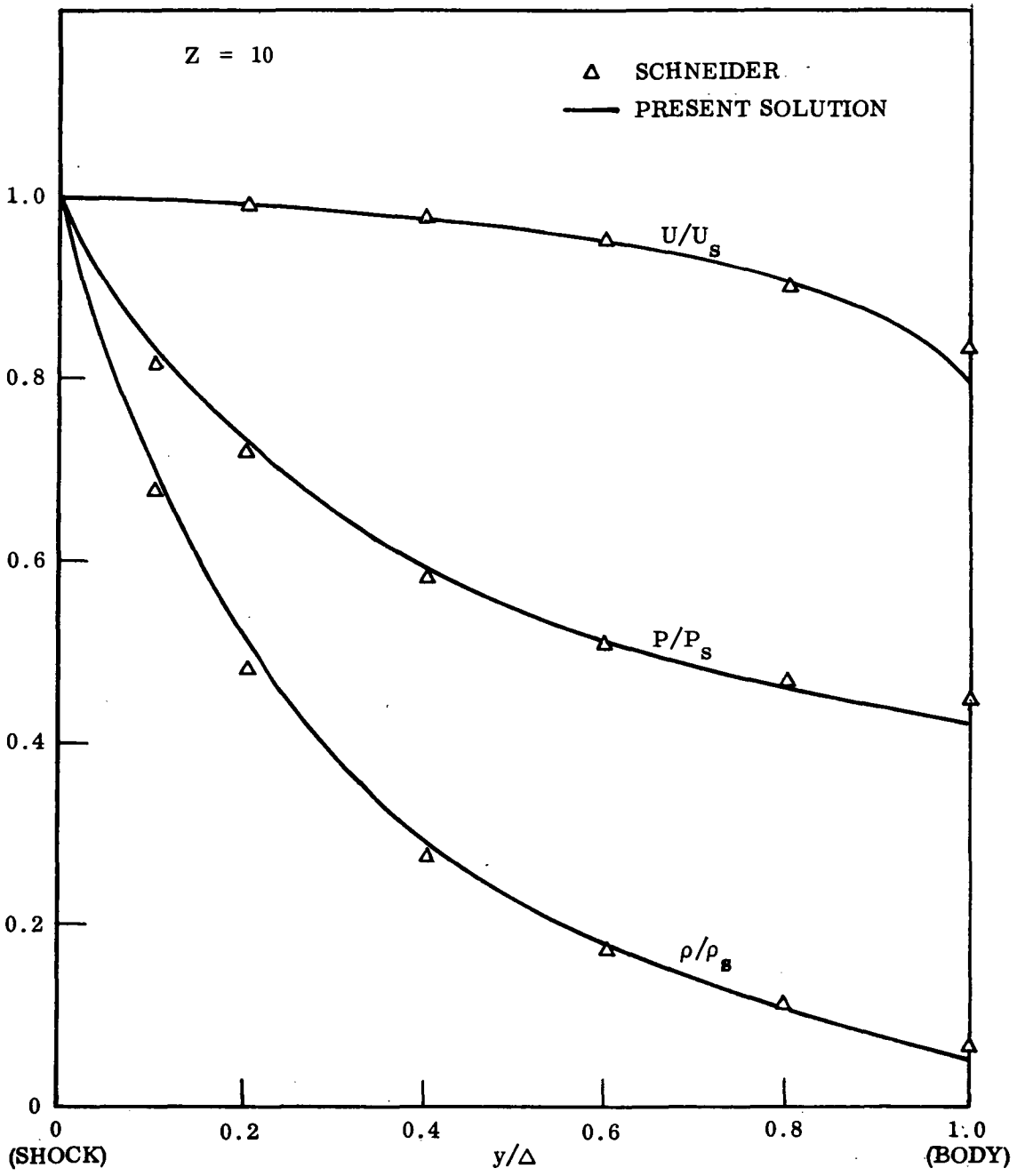


Fig. 4. Profiles Behind a Parabolic Shock

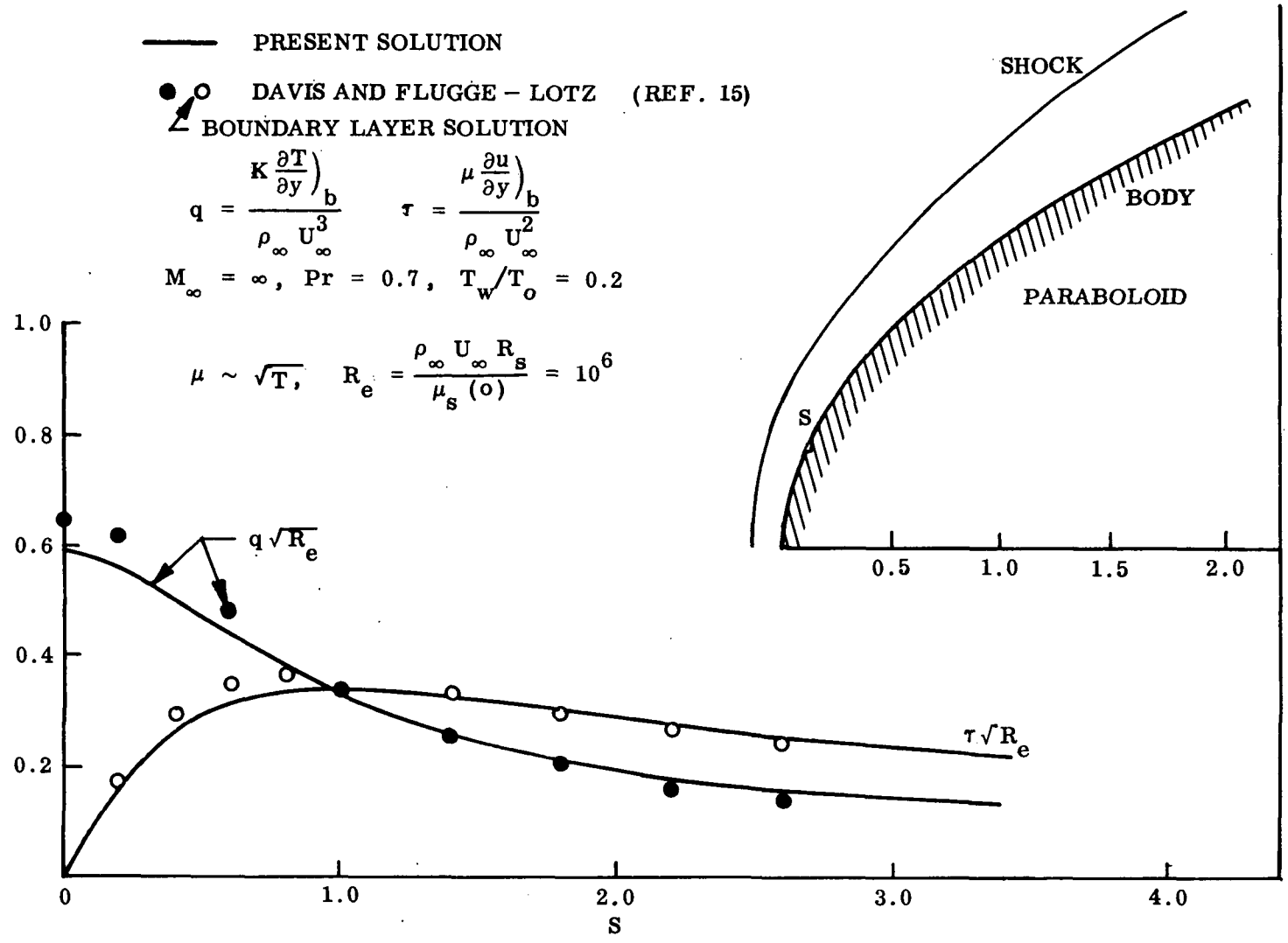


Fig. 5. Convective Heat Flux and Skin Friction Around a Paraboloid at Hypersonic Speed

profiles as the flow flows downstream.

Thermodynamic as well as transport properties are calculated by the extended FEMP routine in this solution. We list the necessary input quantities as follows:

| | |
|---|---|
| Flight Conditions | $\rho_\infty = 4.21 \times 10^{-7}$ gr/cm$^3$ , $u_\infty = 1.6 \times 10^6$ cm/sec |
| Shock Shape | $Z = \dfrac{r_s^2}{2 + 1.19\, r_s}$ |
| Shock Nose Radius | $R_s = 234$ cm |
| Reynolds Number | $Re = 2.48 \times 10^5$ |
| Wall Enthalpy | $H_w = 0.2, \qquad \bar{H}_w = 0$ |
| Surface Mass Injection Rate | $(\rho v)_w = \dfrac{-0.3}{1 + r_s^2}$ |

Atmospherical Gas: Air Injected Gas: Air (41)

The results are plotted in Figs. 6 and 7. Figure 6 shows the shock and body shapes. Also plotted in the figure is the interface between the atmospheric gas and the injected gas. This interface is defined as the surface where the stream function is zero. We see that the body shape is not significantly different from the shock shape. The injected gas layer grows but at a slower pace than the growth of the total shock layer. This is because of the decreasing surface injection rate around the body. Figure 7 shows the tangential velocity and static enthalpy profiles. It is seen that the viscous layer is detached from the wall due to mass injection. Hence, both the convective heat transfer and the skin friction are practically zero. The inviscid layer near the wall becomes thinner as the flow flows far downstream.

5.3 Inviscid Shock Layer with Radiation but without Blowing--Evaluating the $Q_\xi$ Effect

In the derivation of the equation for $\bar{H}$ we have neglected the term

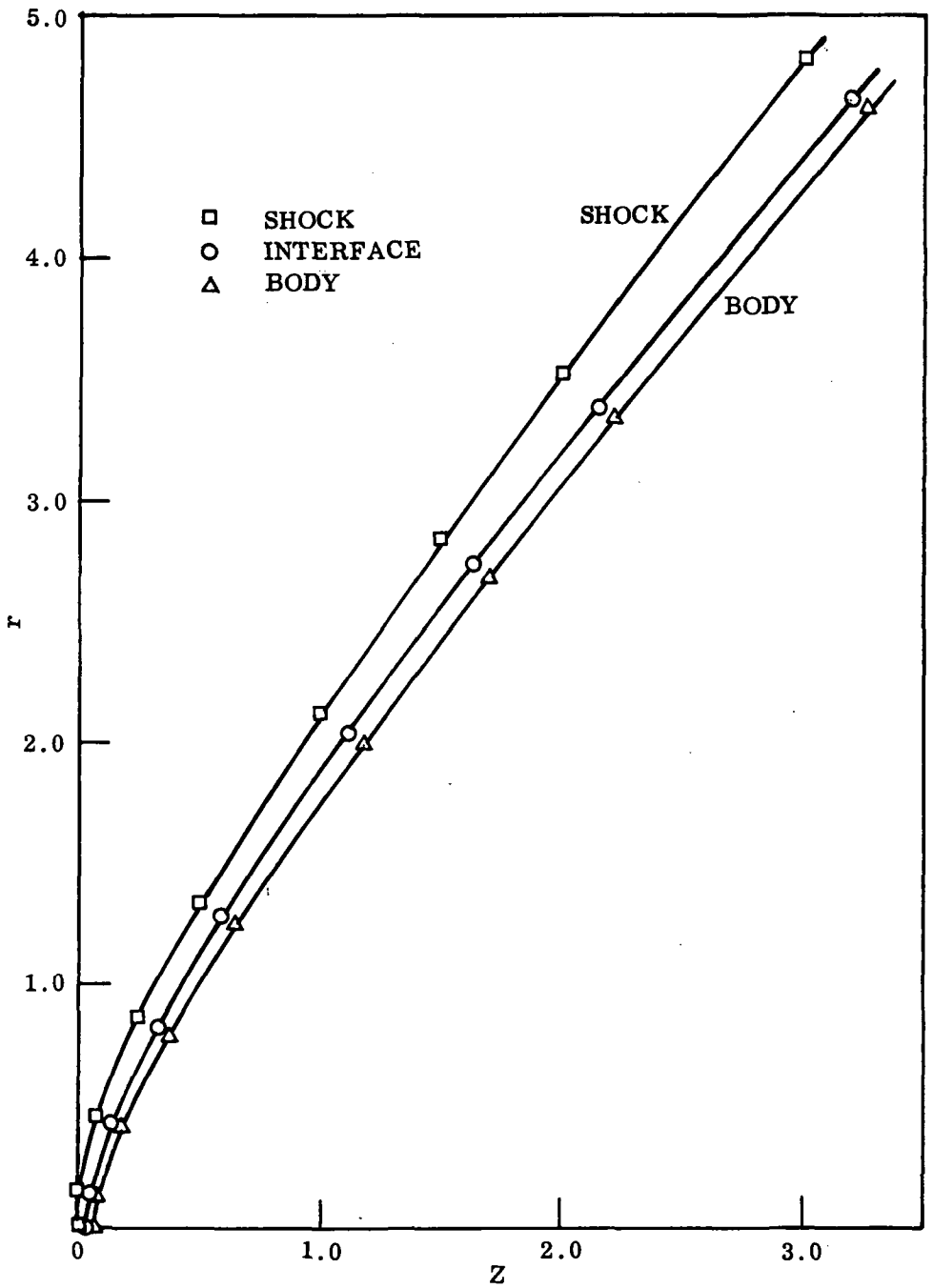


Fig. 6. Shock and Body Shapes for a Blowing Case

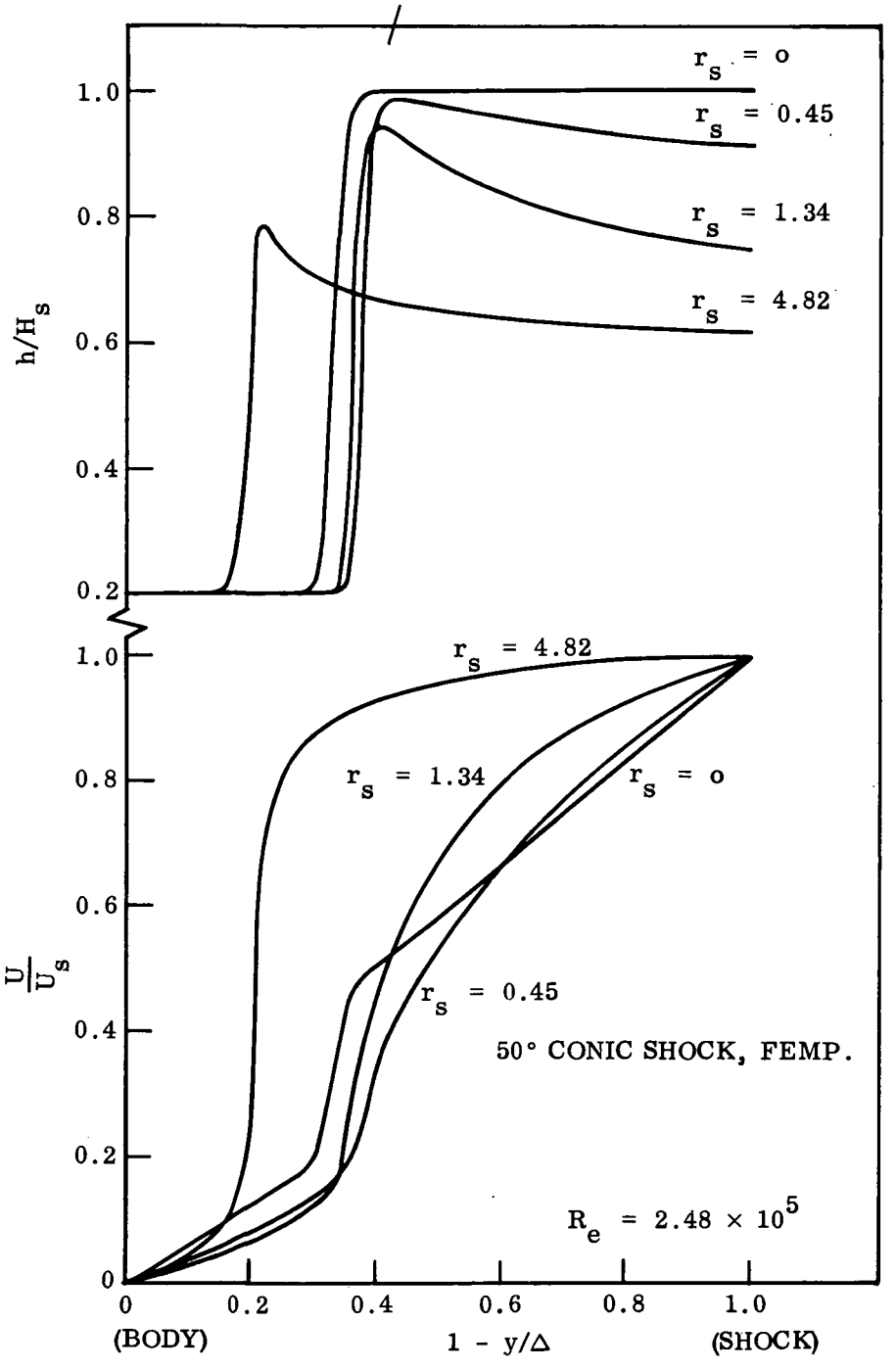


Fig. 7. Enthalpy and Velocity Profiles for a Blowing Case

$\frac{\partial Q}{\partial \xi}$, namely, we have neglected the contribution of the streamwise rate of change of radiative flux divergence to the energy equation. In order to assess the effect of $\frac{\partial Q}{\partial \xi}$ on the radiative wall flux we have made computations with and without this term. The computation is for an inviscid, nonblowing case; the flight condition and shock shape are the same as given by Eq. (41) and the shock nose radius is 100 cm. The three-band radiation transport model for air continuum as described in Ref. 7 is employed for this particular case. Figure 8 shows the result for radiative wall flux, the dotted line is the result for $\frac{\partial Q}{\partial \xi} = 0$, while the solid line represents the result for $\frac{\partial Q}{\partial \xi} \neq 0$. We see that the result for $\frac{\partial Q}{\partial \xi} = 0$ is always higher than for $\frac{\partial Q}{\partial \xi} \neq 0$. The maximum difference between these two results in this case is about 15%. A 15% inaccuracy seems to be reasonable to accept in view of the simplification it will introduce by neglecting this $\frac{\partial Q}{\partial \xi}$ term. To evaluate $\frac{\partial Q}{\partial \xi}$ in the present study would require the $\xi$-derivatives of Eq. (35). It involves, first, the transformation of those equations from $(x,y)$ plane to $(\xi,\eta)$ plane, then taking partial derivatives with $\xi$ by keeping $\eta$ fixed. A tremendous amount of algebraic manipulation would have to be made in this process, and this can all be avoided by simply neglecting $\frac{\partial Q}{\partial \xi}$ in the $\bar{H}$ equation. Although the effect of $\frac{\partial Q}{\partial \xi}$ on the wall flux is not negligible, we have demonstrated for the case of three-band radiation models that the effect is on the conservative side and is reasonably small.

## 5.4 Completely-Coupled Radiating Shock Layer with Blowing

A sample calculation is made for the shock layer problem of a Jupiter probe. The flight conditions, as well as other necessary input data, are listed below:

Flight Conditions: $\rho_\infty = 6.9 \times 10^{-7}$ gr/cm$^3$, $u_\infty = 4 \times 10^6$ cm/sec

Shock Shape: $Z = \frac{r_s^2}{2 + 1.88\, r_s}$

Shock Nose Radius: $R_s = 20$ cm

Wall Temperature: $T_w = 4500$ °K

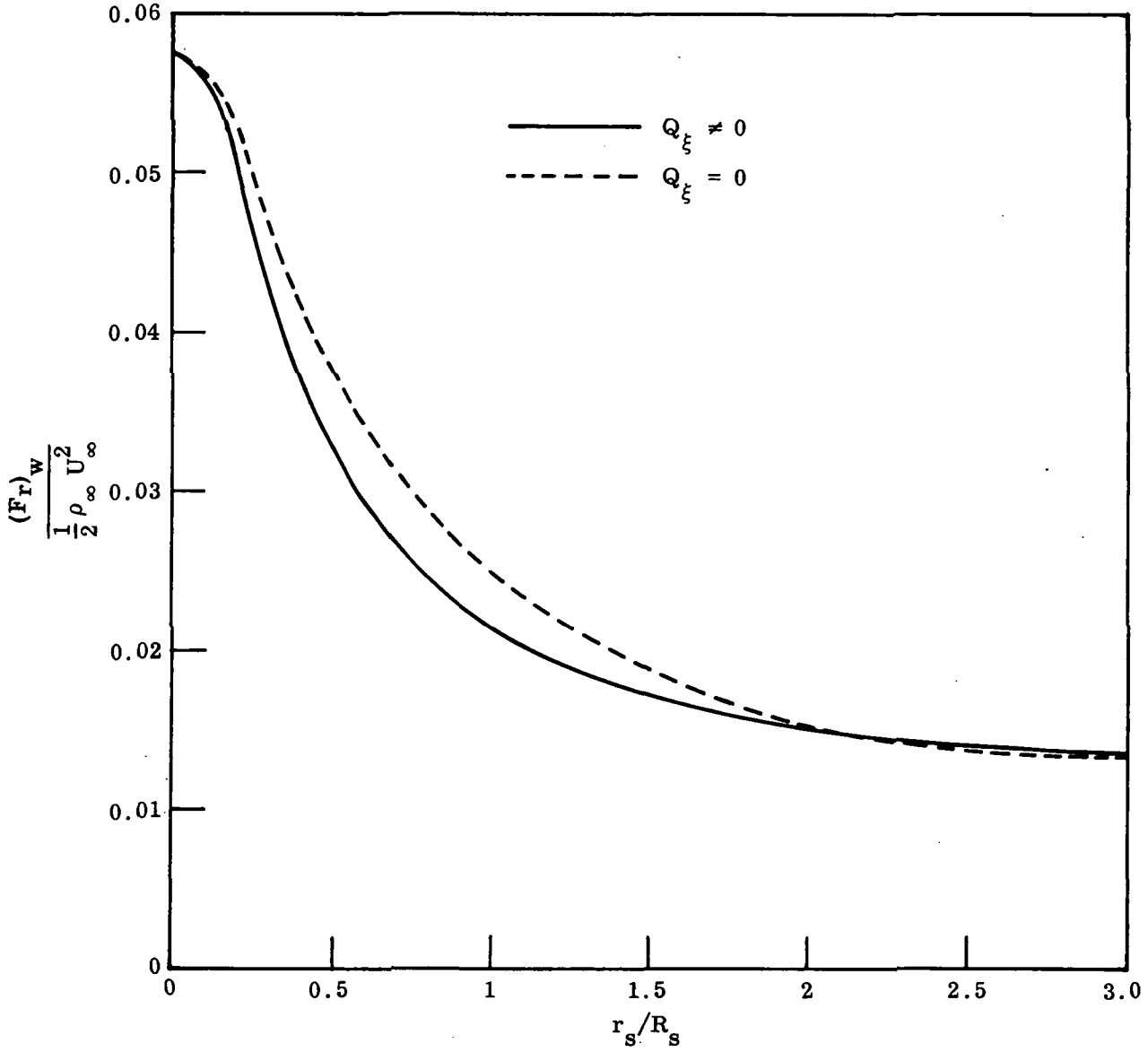


Fig. 8. Effect of Streamwise Derivative of Flux Divergence on the Surface Radiative Flux

Surface Mass Injection Rate $(\rho v)_w = \dfrac{-0.4}{1 + 0.1\, r_s^2}$

Atmospherical Gas: 74% Hydrogen, 26% Helium; by mass. Injected Gas: Carbon
Radiative Model: Given by Refs. 4 and 5.

Based on the flight conditions listed above, the Reynolds number as alculated by FEMP is $9.267 \times 10^4$ and the density ratio $(\rho_\infty/\rho_s)$ across the ormal shock is 0.0964.

In this calculation, the $\xi$-derivatives of the thermodynamic transport uch as $\frac{\partial \mu}{\partial \xi}$, $\frac{\partial Pr}{\partial \xi}$ and $\frac{\partial D}{\partial \xi}$ are neglected for the following two reasons:

(a) Those derivatives turn out to be very sensitive to the local gas omposition [due to the very steep gradient of the ablating product concentration rofile near the interface (the viscous layer)]. This sensitivity causes the teration to become unstable.

(b) The effect of $\frac{\partial \mu}{\partial \xi}$, $\frac{\partial Pr}{\partial \xi}$ and $\frac{\partial D}{\partial \xi}$ should be confined within the viscous ayer; in the present high Reynolds number cases this layer is indeed very hin. Hence, the effect of neglecting $\frac{\partial \mu}{\partial \xi}$, $\frac{\partial Pr}{\partial \xi}$ and $\frac{\partial D}{\partial \xi}$ on the wall radiative lux should be small.

In order to examine the effect of ablation on the radiative wall flux, we also ake a calculation for the nonblowing case. The results are shown in Figs. 9 - 14.

In Fig. 9, the shock shape, body shape, as well as the interface, are shown. The interface is defined as the surface where the stream function is zero. It is found that $R_b/R_s \simeq 0.42$. In the present case, $R_s$ = 20 cm. Hence, the body nose radius of curvature $R_b$ is approximately 8.2 cm. The asymptotic body half cone angle is approximately 57°. Also shown in Fig. 9 is the body shape when there is no blowing. This body shape is practically identical to the interface shape for the blowing case. The last point in the present calculation is at $r_s/R_s \simeq 2$, $r_b/R_s \simeq 1.85$. At this point we see that the shock angle is close to its asymptotic angle which is 62°. Also, we see that, at this point, the shock layer is not exactly a thin layer.

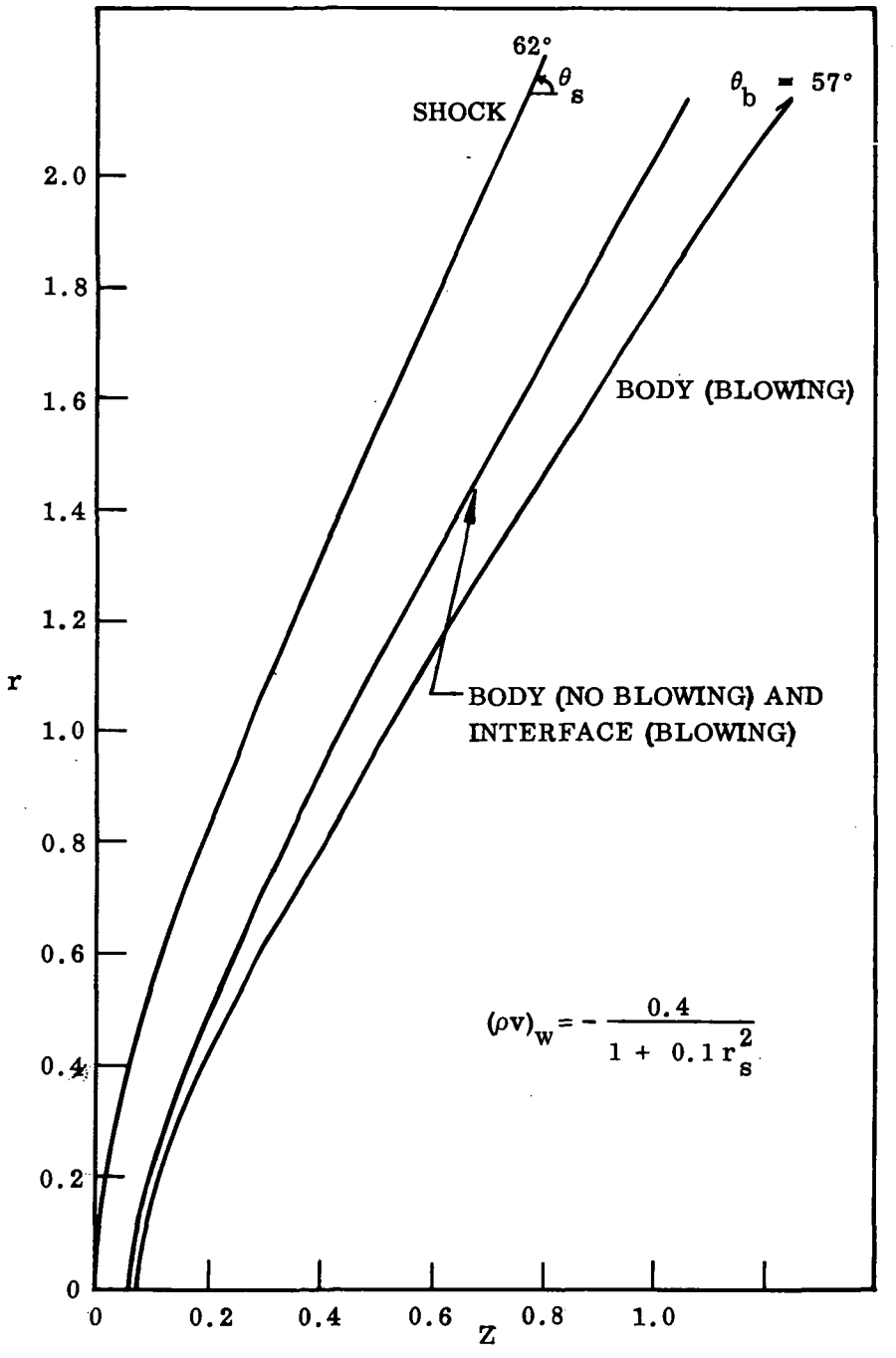


Fig. 9. Shock and Body Shapes for a Radiative Coupled Viscous Shock Layer with Blowing

Figure 10 shows the surface radiative flux for both blowing and no blowing cases. A drastic reduction in radiative flux due to mass injection is seen. The flux distribution for the no blowing case shows an anomalous behavior, namely, the maximum heating is not at the stagnation point. For the present particular case, the downstream flux maintains at a higher level than that at the stagnation point. In order to explain this behavior, we have plotted the shock layer thickness distribution and the temperature profiles in Fig. 11. The shock layer thickness increases rapidly near the nose followed by an almost constant rate downstream. By comparing the temperature profiles at $Z = 0$ and $Z = 0.03$, we see that the temperature changes very little. On the other hand, the shock layer thickness increases by about 40% from 1.2 to 1.8 cm. This results in a higher flux at $Z = 0.03$ than that at $Z = 0$. The temperature decreases as $Z$ increases, but remains at a high level as one can see from the profiles. The decreases in shock layer temperature will result in a lower surface flux, but it is compensated by a thicker shock layer. Hence, the net result is the flux maintains at a nearly constant level which is higher than the stagnation value. For blowing cases, the flux decreases monotonically as can be seen from Fig. 10. The heating level for a blowing case is mostly controlled by the injected gas layer. A monotonically increasing injected gas layer should result in a monotonically decreasing flux distribution. Figure 12 shows the flux reduction due to the mass injection. The reduction ranges from about 40% at stagnation region to about 70% far downstream. This indicates that injected carbon gas is an effective heat shield in the sense that most of the shock layer hot gas is dumped into the wake. A detailed examination of the spectral distribution of surface radiative flux reveals that most of the continuum flux reduction occurs in the carbon molecular bands of $C_2$ and $C_3$. The reduction in line flux is also a significant portion of the total flux reduction. It is interesting to note that from Fig. 10 one sees that at the stagnation point, the line reduction accounts for about 60% of the total flux reduction.

Figure 13 shows the typical profiles for tangential velocity, enthalpy and injected gas mass fraction profiles at $r_s = 1.22$. It is seen that about 35% of the shock layer is an injected gas layer. The shear layer is thin, about 10% of the shock layer. Most of the injected gas layer is inviscid. The temperature profile and the C, $C_2$, $C_3$ concentration profiles are shown in Fig. 14.

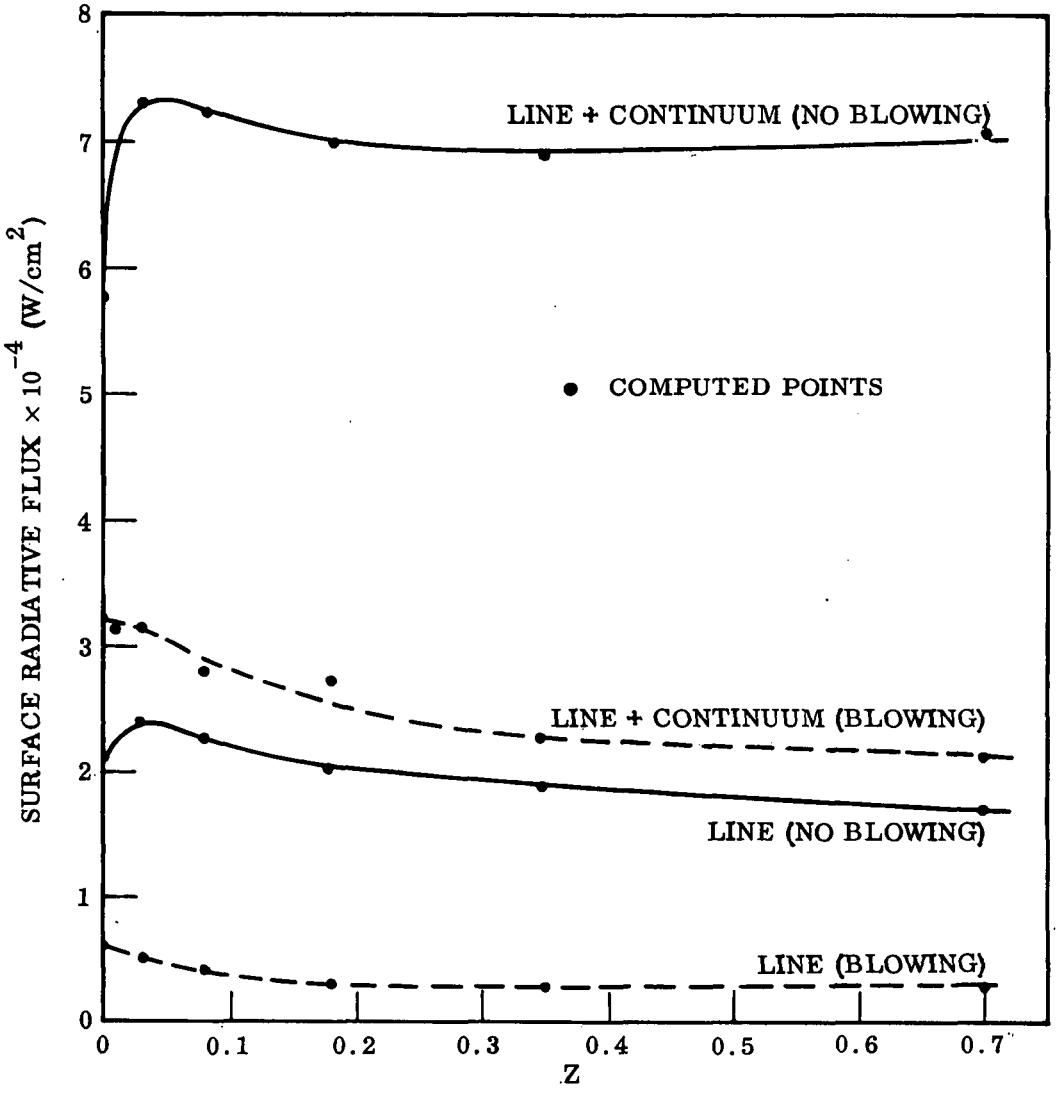


Fig. 10. Surface Radiative Flux for Both Blowing and No Blowing Cases

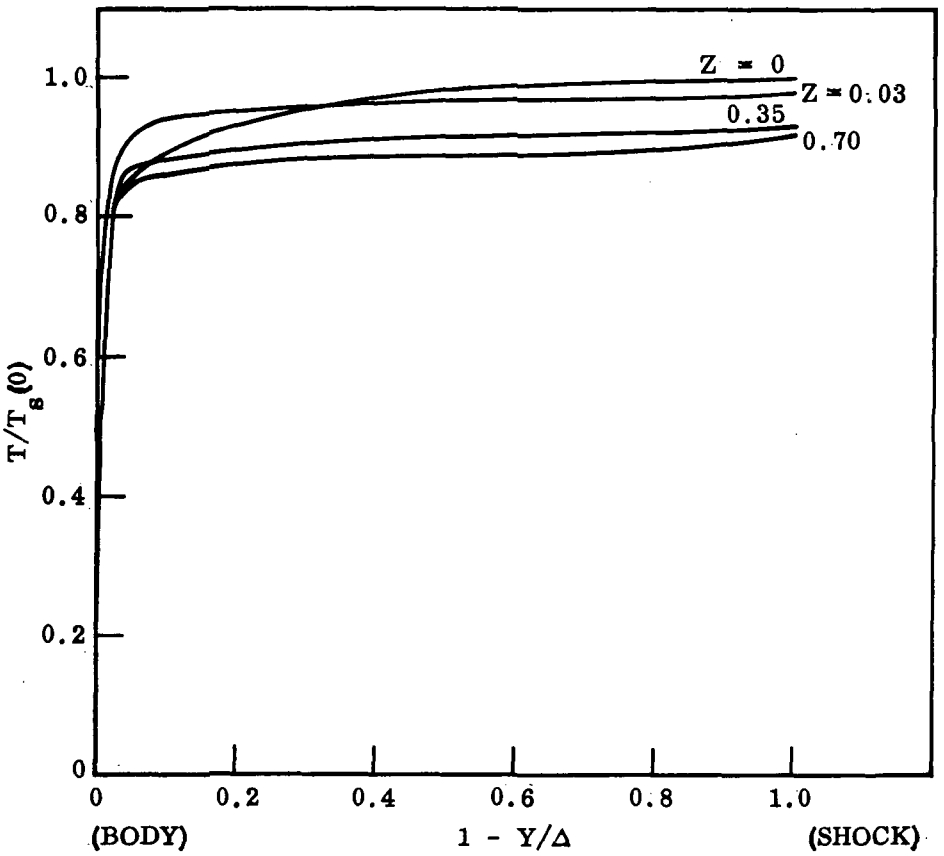


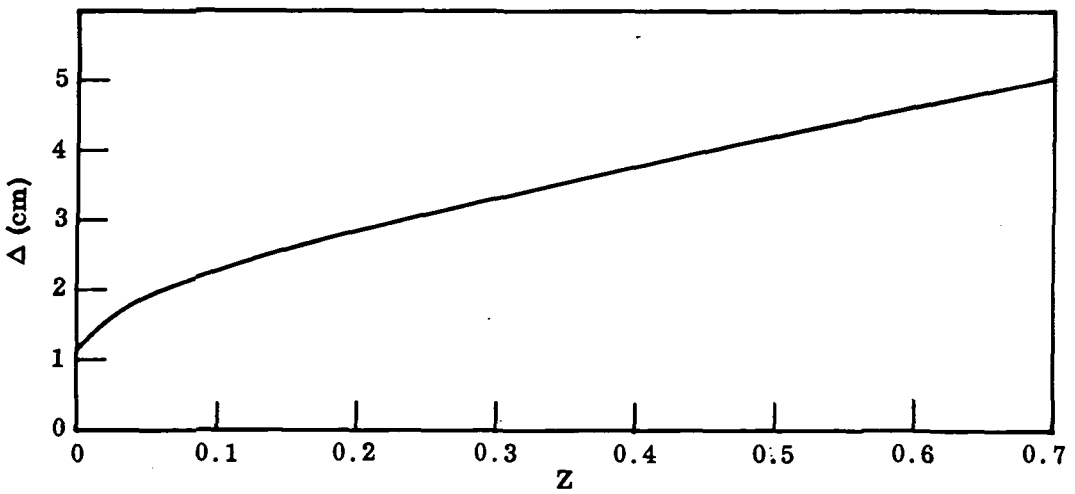


Fig. 11. Shock Layer Thickness and Temperature Profiles for the No Blowing Case

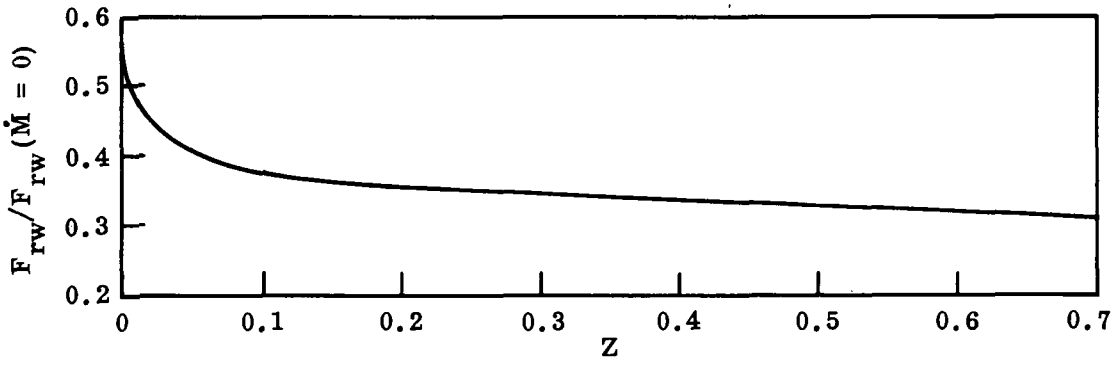


Fig. 12. Surface Flux Reduction Due to Blowing

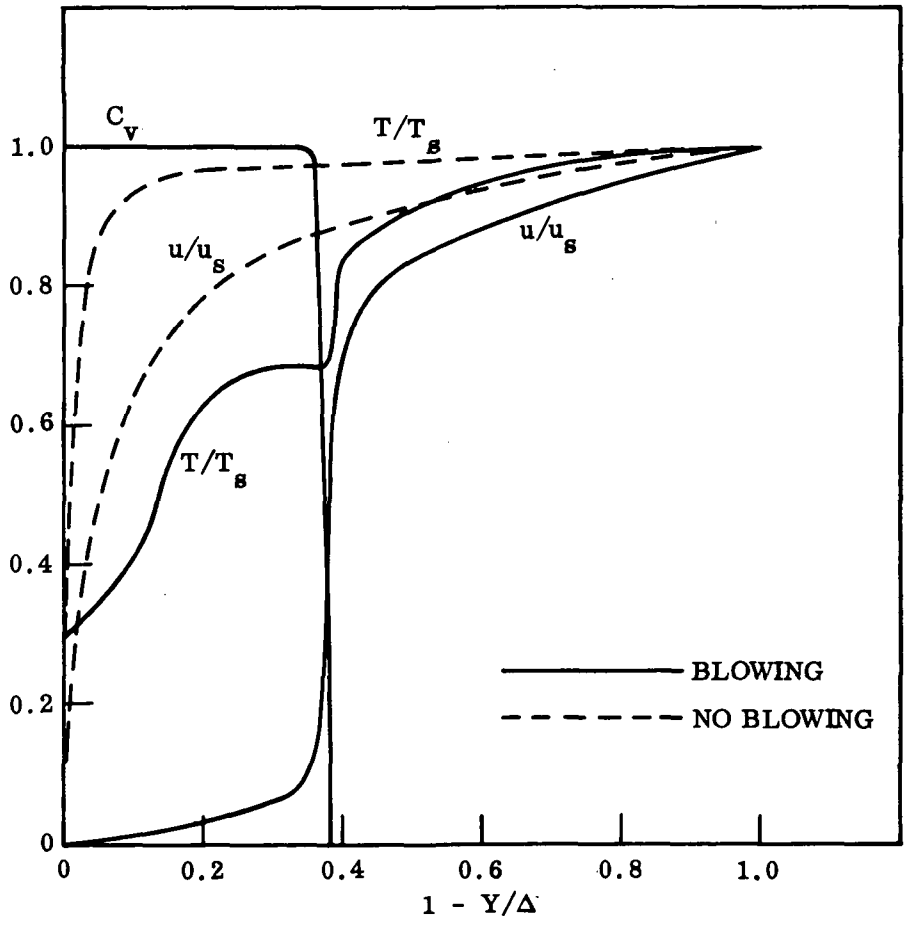


Fig. 13. Temperature, Velocity and Injected Gas Mass Fraction Profiles at Z = 0.35

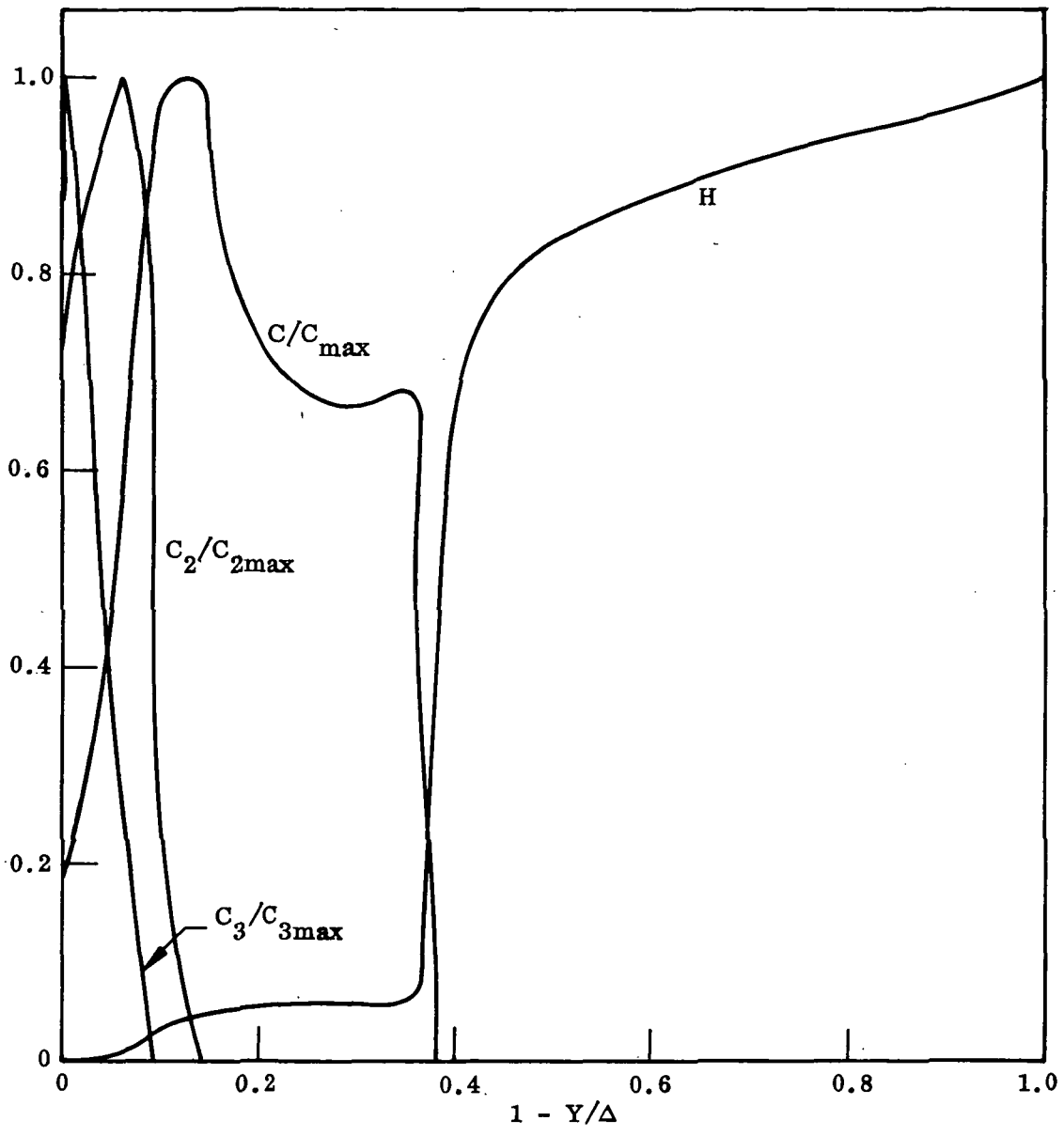


Fig. 14. Enthalpy, $C_1$, $C_2$ and $C_3$ Profiles at Z = 0.35

## 6.0 CONCLUDING REMARKS

Viscous radiating shock layer flow over a blunt body with massive blowing has been solved by a locally nonsimilar approach. Detailed equilibrium computations for the thermodynamic and transport properties are included in the solution. Molecular band and atomic line, as well as continuum radiation, are considered.

Comparisons with prior inviscid solutions for flow behind blunted conic shocks and flow behind parabolic shocks show the present solution method adequately treats nonsimilar aspects of flow around blunt bodies. A sample calculation for a typical Jovian entry problem has been made. A 40% reduction in total radiative flux is found at stagnation point due to the injection of carbon gas. The reduction increases to about 70% at about four body nose radius downstream. This increase of flux reduction indicates that most of the radiative energy is absorbed by the injected carbon gas and dumped into the wake.

An examination of the spectral distribution of the radiative flux reveals that most of the flux reduction occurs in molecular bands of $C_2$ and $C_3$. Due to the large Reynolds number and massive local blowing rate, the solutions indicate that the shear layer remains thin (about 10% of the shock layer). The injected gas layer is mostly inviscid.

Due to the very steep gradient of the ablating product concentration profile near the interface (the viscous layer), the $\xi$-derivatives of the thermodynamic transport such as $\frac{\partial \mu}{\partial \xi}$, $\frac{\partial Pr}{\partial \xi}$ and $\frac{\partial D}{\partial \xi}$ are very sensitive to the local gas composition. This sensitivity causes the iteration in the numerical computation to become unstable. Therefore, in the sample calculation for the Jovian entry problem, $\xi$-derivatives of the thermodynamic transport have been neglected. In the present higher Reynolds number and massive blowing case, the effect of neglecting those derivatives on the wall radiative flux should be small.

## 7.0 REFERENCES


1. Hoshizaki, H. and Lasher, L. E., "Convective and Radiative Heat Transfer to an Ablating Body," AIAA J., Vol. 6, pp. 1441-1449, 1968.

2. Wilson, K. H. and Hoshizaki, H., "Effect of Ablation Product Absorption and Line Transitions on Shock Layer Radiative Transport," NASA CR-1264, Feb. 1969.

3. Chin, J. H., "Radiation Transport for Stagnation Flows Including the Effects of Lines and Ablation Layer, " AIAA J. Vol. 7, No. 7, pp. 1311-1318, July 1969.

4. Wilson, K. H., "Stagnation Point Analysis of Coupled Viscous-Radiating Flow with Massive Blowing," NASA CR-1548, June 1970.

5. Wilson, K. H., "Recent Studies of the Effect of Massive Blowing on Planetary Entry Heating," LMSC Report 4-05-71-8, 1971.

6. Olstad, W. B., "Nongrey Radiating Flow About Smooth Symmetric Bodies," AIAA J. Vol. 9, No. 1, Jan. 1971.

7. Chou, Y. S., "Locally Nonsimilar Solutions for Radiating Shock Layer About Smooth Axisymmetric Bodies," NASA CR-1989, March 1972.

8. Wilson, K. H., "Evaluation of One-Dimensional Approximations for Radiative Transport in Blunt Body Shock Layers, NASA CR-1990, March 1972.

9. Browne, H. N., Williams, M. W. and Cruise, D. R., "The Theoretical Computation of Equilibrium Compositions, Thermodynamic Properties and Performance Characteristics of Propellant Systems," NAWEDS Report 7043, June 1968.

10. Wilke, C. R., "A Viscosity Equation for Gas Mixtures," J. Chem. Physics Vol. 18, No. 4, April 1950, pp. 517-519.

11. Mason, G. A. and Saxena, S. C., "Approximate Formula for the Thermal Conductivity of Gas Mixtures," The Physics of Fluids, Vol. 1, No. 5, Sept.-Oct., 1958, pp. 361-369.

12. Maslen, S. H., "Inviscid Hypersonic Flow Past Smooth Symmetric Bodies," AIAA J., Vol. 2, No. 6, June 1964.

13. Blake, L. H., "Approximate Transport Calculation for High Temperature Air," AIAA J., Vol. 8, No. 9., Sept. 1970, pp. 1698-1700.

14. Schneider, W., "A Uniformly Valid Solution for the Hypersonic Flow Past Blunted Bodies," J. Fluid Mech., Vol. 31, Part 2., 1968, pp. 379-415.

15. Davis, R. T. and Flugge-Lotz, I., "Second Order Boundary-Layer Effects in Hypersonic Flow Past Axisymmetric Blunt Bodies," J. Fluid Mech., Vol. 20, Part 1964, pp. 593-623.

NATIONAL AERONAUTICS AND SPACE ADMINISTRATION
WASHINGTON, D.C. 20546

OFFICIAL BUSINESS
PENALTY FOR PRIVATE USE $300

SPECIAL FOURTH-CLASS RATE
BOOK

POSTAGE AND FEES PAID
NATIONAL AERONAUTICS AND
SPACE ADMINISTRATION
451

U.S.MAIL

POSTMASTER: If Undeliverable (Section 158 Postal Manual) Do Not Return

*"The aeronautical and space activities of the United States shall be conducted so as to contribute . . . to the expansion of human knowledge of phenomena in the atmosphere and space. The Administration shall provide for the widest practicable and appropriate dissemination of information concerning its activities and the results thereof."*

—NATIONAL AERONAUTICS AND SPACE ACT OF 1958

# NASA SCIENTIFIC AND TECHNICAL PUBLICATIONS

TECHNICAL REPORTS: Scientific and technical information considered important, complete, and a lasting contribution to existing knowledge.

TECHNICAL NOTES: Information less broad in scope but nevertheless of importance as a contribution to existing knowledge.

TECHNICAL MEMORANDUMS: Information receiving limited distribution because of preliminary data, security classification, or other reasons. Also includes conference proceedings with either limited or unlimited distribution.

CONTRACTOR REPORTS: Scientific and technical information generated under a NASA contract or grant and considered an important contribution to existing knowledge.

TECHNICAL TRANSLATIONS: Information published in a foreign language considered to merit NASA distribution in English.

SPECIAL PUBLICATIONS: Information derived from or of value to NASA activities. Publications include final reports of major projects, monographs, data compilations, handbooks, sourcebooks, and special bibliographies.

TECHNOLOGY UTILIZATION PUBLICATIONS: Information on technology used by NASA that may be of particular interest in commercial and other non-aerospace applications. Publications include Tech Briefs, Technology Utilization Reports and Technology Surveys.

***Details on the availability of these publications may be obtained from:***

**SCIENTIFIC AND TECHNICAL INFORMATION OFFICE**

**NATIONAL AERONAUTICS AND SPACE ADMINISTRATION**

**Washington, D.C. 20546**